Diabetes-Tuberculosis Comorbidity Characterized by Reduced Type-II Interferon and Elevated Th17 Responses.

Shweta Chaudhary,[1] Mothe Sravya,[1] Falak Pahwa,[1] Sureshkumar V,[2] Prateek Singh,[3] Shivam Chaturvedi,[4] Debasisa Mohanty,[2] Debasis Dash, [3,5] Ranjan Kumar Nanda[1]

[1]Translational Health Group, International Center for Genetic Engineering and Biotechnology, Aruna Asaf Ali Marg, New Delhi

[2]National Institute of Immunology, Aruna Asaf Ali Marg, New Delhi

[3]CSIR-Institute of Genomics and Integrative Biology, Mathura Road Campus, New Delhi

[4]Animal House, International Center for Genetic Engineering and Biotechnology, Aruna Asaf Ali Marg, New Delhi

[5]Institute of Life Sciences, Nalco Nagar Rd, NALCO Square, NALCO Nagar, Chandrasekharpur, Bhubaneswar, Odisha

Highlights

- Elevated serum IL-6, TNF-α, and IL-17A levels reflect hyperinflammation in diabetic mice.
- Lung $CD3^+$ and $CD11c^+$ cell single-cell RNA-seq profiles reveals inflammaging in diabetic mice.
- Fewer lung-infiltrating $CD3^+$ cells in diabetes-tuberculosis (DM-TB) mice suggested delayed immune response.
- Weaker pro-inflammatory response, with reduced Th1/CD4-CTL activity and more Th17-driven tissue damage observed in DM-TB mice.

Summary

Understanding the perturbed lung immune cell distribution and their functionality in tuberculosis is well documented; however, limited reports covered their disruption, if any, in diabetes-tuberculosis (DM-TB) comorbid conditions. Here, we measured serum cytokines and employed single-cell RNA-seq to investigate the molecular mechanisms that govern the heterogeneity in host immune response in DM-TB comorbid conditions. Diabetes associated with chronic hyperinflammation and reduced lung-infiltrating immune cells delayed the immune response to Mycobacterial infection. scRNA-seq of lung $CD3^+$ and $CD11c^+$ cells revealed compromised adaptive and innate immunity, with decreased Th1 and M1 macrophage populations in DM-TB mice. A dampened immune response, marked by increased IL-16 signaling and reduced TNF and IFN-II responses observed in DM-TB. This study highlights chronic inflammation, hyperglycemia, and dyslipidemia associated with diabetes impairing anti-TB immunity, and selective inhibition of aberrant IL-16 secretion and Th17 cell activation might provide strategies for better management of this comorbidity.

Graphical Abstract

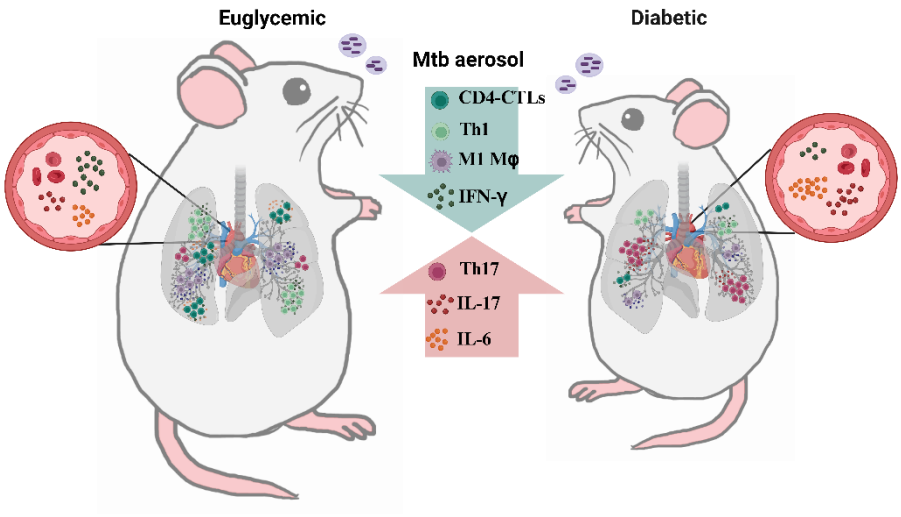

Key words: Diabetes, tuberculosis, scRNA sequencing, immunology, inflammation, T-cell immunity

Introduction:

Tuberculosis (TB) is caused by microorganisms from the *Mycobacterium tuberculosis* (Mtb) complex. Globally, an estimated 10.6 million (95% UI: 9.9–11.4 million) people developed TB in 2022, with ~1.3 (95% UI: 1.18–1.43) million reported deaths.[1] After COVID-19, in 2022, TB remained the second leading cause of death due to a single infectious agent. The five major risk factors for TB include HIV infection, malnutrition, alcohol use disorders, smoking, and diabetes.[1,2] Mtb primarily affects the lungs but can also impact other organs, including the liver, bones, intestines, skin, and lymph nodes..[2]

In 2021, 537 million adults were living with diabetes mellitus (DM) globally, which accounts for one in every ten adults.[3] DM increases the risk of developing active TB disease by three times (95% CI, 2.27-4.46), with six times higher odds of death during treatment.[4] Diabetic patients with TB (DM-TB) also present a higher bacterial burden during case presentation and an increased incidence of cavitary lesions. In addition, the involvement of the lower lung lobe increases in diabetic individuals of ≥40 years of age, leading to misdiagnosis.[4] Diabetic patients report higher baseline IL-6 in addition to increased type 1 and type 17 cytokines.[5] Higher circulatory IL-6 levels at baseline in TB patients are reported to be associated with a heightened risk of treatment failure.[6] Earlier reports in the DM-TB mice model showed a delayed Mtb dissemination, the slow rise of circulatory IFN-γ levels and a low CD14 and MARCO expression in alveolar macrophages (AMϕ).[7-10] The ever-increasing global DM prevalence might lead to a resurgence in TB infections. Therefore, it is crucial to understand the immunological interplay between DM and TB to develop and aid in effective management strategies for DM-TB comorbid conditions. Inferences from the commonly used euglycemic animal models and human subjects having TB might have limited translatability in immunocompromised DM-TB patients. Reports defining the metabolic consequences and lung immune landscape in DM-TB comorbid conditions are scarce. The effect of DM on TB susceptibility, pathogenesis, and progression needs to be studied in a focused way for a better understanding.

The majority of the studies on DM-TB comorbid conditions have been focused on specific subsets of macrophages, NK or T-cells. Earlier reports successfully delineated that the immune landscape of Mtb infected mice and macaque models is complex, involving multiple cell types and extensive intracellular communication.[11-13] Single-cell RNA sequencing (scRNA-seq) provides an opportunity for in-depth profiling of immune cell populations in a model system.

In the current study, we employed nicotinamide-streptozotocin (NA-STZ) based DM induction in C57BL/6 mice and aerosol-infected them with Mtb H37Rv. To understand the immunological heterogeneity in DM-TB comorbid condition at the peak of anti-TB adaptive immune response[14], i.e., 21 days post-infection, in C57BL/6 mice, serum cytokine profiling and 10x Genomics-based scRNA-seq of lung $CD3^+$ and $CD11C^+$ cells from DM-TB and control mice groups (DM, TB, and Healthy) were attempted. Circulatory IL-6, TNF-α, and IL-17A levels were significantly higher in DM-TB and DM groups than in healthy controls. scRNA-seq analysis showed that DM alone induced sterile inflammation and inflammageing in mice lungs. Upon Mtb infection, the DM-TB group showed a delayed immune response, dampened pro-inflammatory Th1, M1 macrophage and CD4+CTLs responses, and heightened Th17-mediated tissue pathology. Collectively, the current study generated resources for further understanding of the lung immune system of diabetic mice and established baseline data to

improve our understanding of the DM-TB comorbid condition. We show that DM-TB comorbidity is associated with the deregulated circulatory cytokine and lung tissue immunological profiles. Disrupted immune response in DM-TB condition increased disease severity in DM-TB mice at later time points.

Results:

NA-STZ induced diabetes in mice mimics human T2DM complications: Patients with diabetes show a higher risk for respiratory infections such as influenza, COVID-19 and TB.[15] However, the mechanism of this increased susceptibility remains understudied. The current study aimed to understand the lung immunological landscape in diabetic and DM-TB comorbid conditions. We used a chemically induced model of type 2 diabetes mellitus (T2DM) as described previously with minor modifications.[9] Diabetes was induced in 8–12 weeks old C57BL/6 male mice using nicotinamide and streptozotocin. Hyperglycemia and body weight of DM-induced and control mice were monitored weekly (Figure 1A). NA-STZ induced mice showed a significant decline in body weight, corroborating earlier literature that reported a loss of body weight upon STZ treatment. However, this loss in body weight subsided after the last NA-STZ dose, and eventually, the animals showed an increased trend in their overall body weight gain (Figure 1 B), and the mice remained hyperglycemic throughout the experiment (Figure 1C). Intraperitoneal glucose tolerance test (ipGTT) and insulin tolerance test (ITT) is regularly employed in mice models to assay glucose intolerance and insulin resistance, respectively, and both are characteristic features of T2DM. In our NA-STZ induced model, diabetic mice showed significantly higher insulin resistance (Figure 1D) and glucose intolerance (Figure 1E) at 4 weeks post-induction, compared to age and sex-matched controls. Dyslipidemia is another well-reported complication of T2DM and is a major risk factor for cardiovascular diseases. The NA-STZ induced diabetic mice showed significantly higher circulatory levels of triglycerides (Figure 1F), total cholesterol, free fatty acids and significant hypoinsulinemia as compared to the euglycemic controls at 11 weeks post-induction (Figure 1F, G, H, I). Hyperglycemia, dyslipidemia, along with insulin resistance and glucose intolerance, indicated that the NA-STZ model in C57BL/6 mice mimics T2DM and its associated complications.

Delayed immune response evident in DM-TB condition: We proceeded with low dose (100-120 CFU) Mtb H37Rv aerosol infection of diabetic mice and euglycemic controls (Figure 2A). At three weeks post-infection, we did not observe a significant alteration in gross tissue pathology for the lung and spleen in either TB or DM-TB groups (Figure 2B, 2C, 2E). However, the lung inflammation score based on hematoxylin and eosin (H&E) stained lung tissue was highest for the DM-TB group (Figure 2D). Cellular infiltration to the lungs was evident in both groups at this time point. However, the inflammation was more dispersed in the lung tissue of the DM-TB group than in euglycemic control (Figure 2D, Supplementary Figure S1). At 3 weeks post-infection, lung and spleen bacterial burden was similar (Figure 2F) in diabetic and control groups, corroborating earlier reports by Cheekatla et al.[9] Since we did not observe any differences in the tissue bacterial burden at early time points, we measured serum pro-inflammatory cytokine levels using LegendPlex™ to monitor any group-specific differences (Figure 2G, Supplementary Figure S2). IFN-γ is a type II interferon released by the Th cells and NK cells, which counteracts microbial infection in the host. IFN-γ activates macrophages by stimulating the production

of reactive nitrogen species. In addition, IFN-γ stimulates macrophages to overcome phagolysosome maturation by activating apoptosis via caspases 3 or 7, thus blocking mycobacterial replication.[16] IFN-γ also prevents hyperinflammation in the lung by limiting excessive neutrophil migration to the site of infection.[16] We observed significantly higher circulatory IFN-γ levels in both TB and DM-TB mice groups compared to the uninfected control, corroborating earlier reports.[17] While the overall IFN-γ levels were lower in the DM-TB compared to the TB group, they were insignificant (Figure 2G). TNF-α is responsible for initiating cytokine response against intracellular pathogens like Mtb by inducing the expression of chemokines like CXCL9 and CXCL10, which facilitate T-cell recruitment at the site of infection.[18,19] TNF-α is reported to be associated with insulin resistance development in T2DM individuals.[20] Reports showed higher circulatory levels of pro-inflammatory cytokines such as TNF-α, IL-6 and IL-1β in T2DM patients and experimental mice models.[6,9,21] We observed significantly higher circulatory TNF-α levels in DM, TB and DM-TB conditions compared to healthy controls, while IL-6 and IL-17A levels were elevated in DM and DM-TB conditions (Figure 2G). Earlier reports showed that in mice models of DM-TB, higher IL-6 levels damage the lung tissue, resulting in immune pathology in these animals.[9] Higher IL-6 levels in DM-TB comorbid patients before treatment are associated with worsened treatment outcomes.[6] Increased IL-17A levels in newly diagnosed T2DM patients have been reported, and the circulatory IL-17A levels positively correlate with TNF-α levels.[22] In this study, we report significantly higher circulatory IL-6, IL-17A and TNF-α levels in TB and DM-TB groups, corroborating earlier reports.[17]

Macrophages, dendritic cells and T-cells are the key players during early events of Mtb infection. Alveolar macrophages present Mtb with a preferred niche, and the pathogen is known to delay antigen presentation by both macrophages and dendritic cells at the nearby draining lymph node. It is well demonstrated in the literature that the immune response against Mtb starts in the draining lymph nodes and not in the lungs.[23] Therefore, macrophages and dendritic cells are crucial in disseminating the pathogen to initiate host defence. T cells are well known for their anti-TB responses. A three-day slower Mtb dissemination was reported in diabetic mice than in euglycemic controls, leading to a delayed initiation of the immune response.[7] Reports show that 21 days post Mtb infection is the peak of immune response in C57BL/6 mice.[14] Thus, we decided to study anti-TB response in diabetic mice and controls at this crucial time. We flow-sorted $CD11c^+$ (DCs, macrophages and resident monocytes) and $CD3^+$ (T and NK cells) cells from the lungs of TB, DM-TB, DM and healthy mice (Figure 2H). We observed that while infection with Mtb H37Rv led to a significant increase in lung $CD11c^+$ and $CD3^+$ populations in both DM-TB and TB mice compared to healthy controls, the overall frequency of $CD3^+$ cells was significantly lower in the DM-TB group when compared to Mtb infected euglycemic controls (Figure 2I). Similarly, the overall reduction in $CD11c^+$ cells was observed in DM-TB mice compared to TB controls but was statistically insignificant (Figure 2I). Therefore, these observations suggest that while the difference in lung bacterial burden may not be significant in the DM-TB group, there were clear differences at the immunological scale.

Single-cell RNAseq profile of diabetic lung: To characterize the lung immune cell landscape of diabetic mice and euglycemic controls, we performed 10x Genomics scRNAseq of paraformaldehyde-

fixed samples (Figure 3A). Following single-cell alignment and quality control steps, 5,364 and 7,838 CD3+ and Cd11c+ lung cells from healthy and DM groups respectively, qualified the criteria (Supplementary Figure S3). While the average number of high-quality cells captured for the DM group was higher than that of the healthy group, the total lung cell count was similar. Based on canonical gene expression, we identified 3 major cell types: T-cells (*Cd3d+*), B-cells (*Ms4a1+*) and myeloid cells (*Cd14+ Itgam+, Itgax+*) (Figure 3B). Since we did not selectively sort for B-cells, the number of cells in this cluster was quite low, and excluded from further analysis. Upon comparing the healthy and DM groups, we identified 14 cell types, with eight subtypes in the T cell cluster and six subtypes in the myeloid cell cluster. T cell subcluster included Naïve CD4+ T cells (Cd4+ Sell+ Ccr7+), Naïve CD8+ cells (Cd8a+ Sell+ Ccr7+), Th1 cells (Cd4+ Tbx21+ Ifng+), Th17 (Cd4+ Rorc+ Il17a+ Il23r+), Treg (Cd4+ Foxp3+ Ctla4+), Tfh (Bcl6+ Maf+ Cxcr5+), CD4 CTLs (Cd4+ Mki67+ Gzmk+ Gzma+) and CD160+ NKT cells (Cd3d+ Cd8a+ Nkg7+ Klrd1+). The lung myeloid cell compartment was composed of AMφ (Marco+ Siglecf+), pDC (Bst2+ Siglech+), mDC (Ifi30+ Flot1+ Psmb9+), cDC1 (Xcr1+ Cd24a+ Clec9a+), classical monocytes (Cd14+ Fcgr3- Sell+ Ccr2+) and intermediate monocytes (Cd14+ Fcgr3+ Treml4+ Sell+) (Figure 3C). Each subtype was identified based on the expression of known markers (Figure 3D). We observed that the overall proportion of Th17 cells was higher in the lungs of diabetic mice as compared to healthy controls (Figure 3E). Increased Th17 cell numbers have been implicated in inflammageing associated chronic diseases such as T2DM. In addition, we observed that the number of naïve CD4+ T cells was higher in DM mice lungs than in healthy controls (Figure 3E). The scRNAseq analysis of lung immune cells from diabetic mice revealed a dysregulated immune cell composition characterized by an elevated frequency of naïve CD4+ T-cells and inflammatory Th17 cells.

T-cells of diabetic mice showed altered gene expression patterns: The overall number of Tfh, Th1, Th17, Tregs, and naïve CD4+ T cells was higher in the DM group than in the healthy control (Figure 3E). We performed DeSeq2 analysis for naïve CD4+ T-cells to understand the perturbation in functionality of these cells in their inactive baseline state. A set of 320 differentially expressed genes (DEGs, $\log_2 FC > \pm 1.0$, $p < 0.05$) in naïve CD4+ T cells of the DM group were identified, out of which gene expression for 88 genes was downregulated and 232 genes upregulated (Figure 4A). Gene set enrichment analysis (GSEA) for biological processes of the upregulated genes showed enrichment of type 1 interferon responses, inflammasome-mediated signalling, pyroptosis, IL-1 production, T-cell proliferation, and innate immune responses. NLRP3 inflammasome activation is associated with IL-1β release and pyroptosis (Supplementary Figure S4). Pyroptosis has been implicated in sterile inflammatory diseases, particularly in T2DM and lung inflammation in asthma. Reports show that NLRP3 inflammasome-mediated pyroptosis contributed to islet inflammation in T2DM patients and chemically induced diabetic rat models[24]. This study shows that NLRP3 mediated pyroptosis is not limited to pancreatic islet cells and induces a sterile inflammatory state in the lung of T2DM mice models. Type 1 interferon responses have an antagonistic effect on IL-1 responses, and IFN-β has been known to suppress IL-1 transcription and translation.[25] In the case of DM mice, IFN-β appears to be playing an anti-inflammatory role by limiting IL-1 driven immunopathology. The negatively enriched pathways in naïve T-cells in the DM group majorly belong to the regulation of biochemical pathways, such as glucose, fatty acid, organic acid, prostaglandin transport, triglyceride, fructose-6-phosphate, glutamine,

and long-chain fatty acyl CoA metabolism (Supplementary Figure S4). These metabolic pathways support the energy need and overall metabolic flexibility of naïve T cells, ensuring they are prepared for activation. Downregulation of genes involved in these metabolic pathways points towards a dysregulated metabolic state of naïve CD4+ T cells in the DM group, which might affect the functionality of these cells upon antigenic stimulation. These results suggest a dysregulated naïve T-cell function in diabetic mice, marked by impaired metabolic regulation and an enhanced inflammatory state.

Decoding lung immune cell transcription regulation in diabetes: We employed single-cell regulatory network inference and clustering (SCENIC) analysis to understand transcription factor dynamics across cell types present in the lungs of DM mice (Figure 4B, Supplementary Figure S4). Klf3, Zfp281 and Foxo1 transcription module activity was specifically suppressed in immune cells from the diabetic group (Figure 4B). Klf3 predominantly functions as a transcription repressor and is known to maintain T-cell quiescence. Klf3 knockout leads to myeloproliferative disorder and systemic inflammation in mice models.[26] Lymphocytes from the DM group, namely, naïve CD4+ T-cells, naïve CD8+ T cells, Tfh, Th1, Th17, Tregs and NKT Cd160+ cells, showed a reduced Klf3 regulation as compared to healthy controls, which is indicative of the activated state of these cells. Zfp281 regulates CD4+ T cell activation and cytokine production by repressing Ctla-4 transcription.[27] Zfp281 knockouts are reported to be present with impaired T-cell activation and cytokine production. While Zfp281 knockdown does not affect T-cell development, it has been reported to impair CD4+ T-cell activation and cytokine production in response to intracellular pathogens, such as *Listeria monocytogenes*.[27] We observed a repressed activity of Zfp281 regulon in the DM group compared to healthy controls (Figure 4B). Forkhead box O (Foxo) family of proteins in T-cells are responsible for various functions like T-cell survival, trafficking, differentiation and memory response. Foxo activity is reported to be inversely proportional to senescence. Foxo1 expression is highest in cord blood cells and, upon ageing, gets diminished in T cell subsets.[28] We observed a diminished activity of Foxo1 in all T-cell subtypes (naïve CD4+, Naïve CD8+, Th1, Th17, Treg and Tfh cells) in the lung of the DM group (Figure 4B), indicating impaired functionality of these cells. Consequently, reduced Klf3 expression in T-cells from the DM group indicates a heightened activation state and loss of quiescence, even without a pathogenic challenge. Meanwhile, reduced Foxo1 activity supports the inflammaging phenotype observed in the lungs of diabetic mice.

Impact of hyperglycemia on pulmonary inflammation: Upon comparing the total number of interactions for cell-cell communication inferred via CellChat analysis, an overall increase in the cellular interaction amongst the DM group was observed (Supplementary Figure S5). The differential strength of interactions was increased in the DM group compared to the healthy control (Figure 4C). In the lungs of diabetic mice, cell signalling mediated by CD4+ CTLs, Tregs, Th1, naïve T-cell and intermediate monocytes was relatively increased. In contrast, signals sent by mDCs, naïve CD8 T-cells and Tfh cells were decreased in DM mice compared to the healthy group (Figure 4C). To further investigate the ligand-receptor interactions specifically deregulated in each group, we compared the overall information flow of each signalling pathway for all study groups. MIF, IL16, FLT3 and LIGHT signalling pathways were significantly enriched in the lungs of DM mice (Figure 4D). Upon further investigating the sender-

receiver dynamics, we observed that while in healthy mice, CD4+ CTLs were majorly responsible for MIF release, in the DM group, both lymphoid (CD4+ CTLs, Naïve CD8+, NKT CD160+ and Th17 cells) and myeloid (alveolar macrophages) population were involved in sending MIF signals (Supplementary Figure S5). MIF is a lymphokine involved in immunoregulation and inflammation. The inflammatory activity of MIF is mediated by its ability to promote pro-inflammatory cytokines such as TNF-α, IL-1β and IL-6. In addition, MIF also overrides the anti-inflammatory effects of glucocorticoids.[29,30] IL-16 is a pro-inflammatory cytokine that works as a chemoattractant for CD4+ cells (T-cells, eosinophils and dendritic cells), prevents antigen-stimulated cell death and prime T-cell activity via IL-2.

IL-16 has also been implicated in airway inflammation in the C57BL/6 model for asthma.[31] We observed an increased IL-16-mediated cellular crosstalk in the DM group (Figure 4E). CD8+ T cells produce IL-16 in response to an antigenic stimulus, while CD4+ T cells have been reported to have a constitutive expression of pro-IL-16 molecule, which gets cleaved upon activation. We observed that Th17 and naïve CD8+ T-cell-based IL-16 interactions were unique to the DM condition. Similarly, cDC1, pDC, and intermediate monocyte-based interactions were also unique for the lungs of diabetic mice. The lymphocyte chemotactic ability of DCs has been reported to be IL-16 mediated. LIGHT is a member of the TNF superfamily and stimulates the growth and activation of T-cells. LIGHT has also been implicated in the pathology of T2DM and is responsible for attenuating insulin release, mediating vascular inflammation and regulating glucose metabolism via GLUT4 expression and signaling for this ligand was specifically enriched in the DM group only (Figure 4D).[32,33] The enhanced signaling of MIF and IL-16 in the lungs of diabetic mice indicates a more pronounced basal inflammatory state within the system. The upregulation in pro-inflammatory signaling points to a chronic, underlying inflammation that may contribute to or exacerbate the overall immune dysfunction observed in diabetes.

Immune cell dynamics in the lungs of diabetes-tuberculosis comorbid condition: A similar bioinformatics pipeline was employed to filter the data sets, of Mtb infected eu- and hyper-glycemic groups based on earlier defined QC parameters, were integrated (Figure 5A). Post single cell alignment and quality control steps, 5,747 and 5,888 cells from TB and DM-TB groups qualified for the criteria (Supplementary Figure S3). Three major cell types in the integrated TB and DM-TB dataset were identified, namely, T-cells (Cd3d+), B-cells (Ms4a1+) and myeloid cells (Cd14+ Itgam+ Itgax+) (Figure 5B). Upon further classification, we identified 15 cell types, with 8 subtypes in the T cell cluster and 7 in the myeloid cell cluster. The T cell subcluster included Naïve CD4+ T cells (Cd4+ Sell+ Ccr7+), Naïve CD8+ cells (Cd8a+ Sell+ Ccr7+), Th1 cells (Cd4+ Tbx21+ Ifng+), Th17 (Cd4+ Rorc+ Il17a+ Il23r+), Treg (Cd4+ Foxp3+ Ctla4+), Tfh (Bcl6+ Maf+ Cxcr5+), CD4 CTLs (Cd4+ Mki67+ Gzmk+ Gzma+) and CD8+ effector T cells (Cd3d+ Cd8a+ Prf1+ Gzmb+). The lung myeloid cell compartment was composed of AMφ (Marco+ Siglecf+), pDC (Bst2+ Siglech+), mDC (Ifi30+ Flot1+ Psmb9+), cDC1 (Xcr1+ Cd24a+ Clec9a+), intermediate monocytes (Cd14+ Fcgr3+ Treml4+ Sell+), NK Cd160+ (Tyrobp+ Nkg7+ CD160+ Klrk+) and M1 macrophages (Itgam+, Cd68+, Nos2+, Tlr2+) (Figure 5C). Each cell subtype identification was based on the expression of canonical markers (Figure 5D, Supplementary Figure S6, S7). We observed that the overall proportion of naïve CD4+, naïve CD8+, Th17 cells and AMφ was higher in the lungs of DM-TB mice. In contrast, the CD4+ CTLs, Th1 cells, intermediate monocytes, and

M1 macrophages were lower than those of the TB group (Figure 5E). scRNAseq analysis of lung immune cells from *Mtb* infected diabetic mice showed a dysregulated anti-TB response, with increased naïve CD4+ and CD8+ T-cells and decreased pro-inflammatory CD4+ CTLs, M1 Mϕ, and Th1 cells.

Differential gene expression highlights dysfunctional T-cells in the lungs of diabetes-tuberculosis comorbidity: The overall number of M1 macrophages, Th1 and CD4 CTLs was lower in DM-TB lungs, while Th17, alveolar macrophages, naïve CD4+ and naïve CD8+ T cells were higher as compared to TB group. Thus, we proceeded with DeSeq2 analysis of these cell subsets (Figure 6A, Supplementary Figure S10). A set of 1,631 DEGs in M1 macrophages of the DM-TB group was identified, out of which 922 genes were downregulated and 709 genes were upregulated (Figure 6A). GSEA for biological processes of the upregulated genes showed enrichment of nitric oxide (NO) mediated signal transduction, regulation of autophagy, response to glucocorticoid stimulus, negative regulation of cell-substrate adhesion, TGF-β signalling pathway and hematopoietic stem cell homeostasis (Supplementary Figure S10). The genes that regulate peptide cross-linking pathways included Thbs1, Stfa3, Fn1 and F13a1. Thbs1, Fn1 and F13a1 are involved in the modulation of extracellular matrix and are correlated with reduced macrophage inflammatory potential, further corroborated by the positive enrichment of TGFβ signalling.[34-37] M1 macrophages of the DM-TB group had significantly higher Trem2, Dapk1 and Bmf gene expression. While Trem2 and Dapk1 positively regulate autophagy, Bmf promotes cell survival, thereby negatively regulating autophagy. Negatively enriched GO terms for DM-TB M1 macrophages included responses to type-I and type-II interferons, AIM2 inflammasome complex assembly, TLR9 signalling pathway, regulation of Th1 responses, pathogen recognition receptor signalling, and innate (NK cell-mediated) as well as adaptive (B cell and Th1 cell-mediated) immune responses (Supplementary Figure S10).

The CD4+ CTLs from the lung of the DM-TB group had 728 DEGs with 324 downregulated genes and 404 upregulated genes (Supplementary Figure S10). CD4+ CTLs from the lung of the DM group showed activated T-cell homeostatic processes, negative regulation of wound healing and regulation of T-cell apoptotic processes. In addition, pathways like nitric oxide-mediated signalling, glycoprotein metabolic process, and response to copper and zinc ions were also positively enriched. In contrast, processes like pyroptosis, defence response to bacteria, complement activation, and response to IL-1β and IFN-β were suppressed in CD4+ CTLs for the DM-TB group (Supplementary Figure S10). Pyroptosis is a form of planned cell death and one of the host mechanisms to control Mtb infection. A suppressed expression of genes involved in complement activation, pyroptosis, leukocyte degranulation and neutrophil activation in CD4+ CTLs points towards a compromised immune response in DM-TB condition.

Transcriptional regulation of lung immune cells in diabetes and tuberculosis comorbid condition: SCENIC analysis of lung immune cells from DM-TB and TB groups showed that Ikzf1, Elk4 regulon activity was suppressed (Figure 6B, Supplementary Figure S11). In contrast, Gata1 and Zic5 regulons were activated in naïve CD8+ and naïve CD4+ cells of DM-TB group (Figure 6B). The Ikzf1 gene is translated to protein Ikaros, which plays a crucial role in T-cell differentiation and early T-cell activation, while Elk4 is important for T-cell activation and immune response upon TCR engagement.[38-

[40] Downregulation of these transcriptional pathways could indicate dysfunctional T-cell differentiation and activation in DM-TB conditions. Stat3 is required for T-cell differentiation into Th17 and Tfh cells. Stat3 also has an anti-apoptotic effect on T cells and aids T-cell proliferation and memory formation. In low glucose environments, STAT3 is activated, which promotes FAO, whereas in high glucose environments, STAT3 is inhibited.[41] We observed suppression of Stat3 activity across all cell types identified in DM-TB (Figure 6B). Nfkb2 and non-canonical NF-κB signalling mediator Relb activities were downregulated in myeloid cells (AMϕ, cDc1, intermediate monocytes, M1 macrophages, mDCs and pDCs) of the DM-TB group (Figure 6B). NF-κB2 and its' downstream regulator Relb facilitate activation of antigen-specific T-cells. Relb helps dendritic cells activate T-cells via antigen presentation and non-conventional cross-priming pathway.[42,43] Elevated Relb expression is also correlated with DC maturation. Atf1 and Ctcf regulon activity was also suppressed in all T cell subtypes (CD4+ CTLs, naïve CD4+ T cells, naïve CD8+ T cells, Tfh, Th1, Th17 and Treg cells) of the DM-TB group (Figure 6B). The consistent downregulation of these transcription factors in the DM-TB group indicates a defective functional state of lung immune cells with impaired DC maturity, antigen presentation, impaired T-cell survival, differentiation and a loss of quiescence in naïve T-cells.

Disrupted cell-cell interactions in diabetes and tuberculosis comorbid condition: Compared to uninfected controls (DM and healthy), both DM-TB and TB groups had an increase in overall cell-cell interaction (Figure 6C, Supplementary Figure S5, S12). However, the DM-TB group had more cell-cell communication interactions than the TB group (Supplementary Figure S11). The strength of interactions in the DM-TB group was also altered compared to the TB group, evidenced by the red/blue-coloured edges in the circle plot representing increased/decreased strength of the interaction in the DM-TB group, respectively, compared to TB controls. In DM-TB comorbid conditions, cell signalling was relatively increased by myeloid DCs, classical DCs, CD4+ CTLs, Th1, Tfh, plasmacytoid DCs, and naïve CD4+ T cells. In contrast, signals sent by M1 macrophages, intermediate monocytes, CD8+ effector T cells, alveolar macrophages, regulatory T-cells, Th17 cells, NK CD160+ cells and naïve CD8 T-cells were lower as compared to the TB group (Supplementary Figure S12). Comparing the overall information flow of each signalling pathway for DM-TB and TB groups revealed that IL-6, IL-16, TWEAK, RANKL, OX40 and CD137 were significantly enriched in the lung immune cells of DM-TB mice (Figure 6D). In contrast, TNF, CD40, IFN-II, COMPLEMENT, CXCL, and LIGHT signalling were significantly higher in the TB group (Figure 6D). Upon exploring the outgoing signals individually for DM-TB and TB groups, we observed that M1 macrophages contributed majorly towards TWEAK-mediated signalling while OX40 and IL-6 signalling was mediated by mDCs (Supplementary Figure S12). Tfh and Th17 cells from the DM-TB group mediated RANKL signals, while TWEAK, OX40, IL-6 and RANKL-mediated communication were completely absent in the TB group (Supplementary Figure S12). Mtb hijacks host IL-16 to facilitate its' intracellular growth.[44] While IL-16 signalling was observed in both DM-TB and TB groups, there was a significant increase in IL-16 mediated signalling for the DM-TB group (Supplementary Figure S11), which is evident in the cell circle plot as well where the edge thickness representing signalling strength is higher for DM-TB dataset (Supplementary Figure S12). Mtb infection is associated with elevated IL-1, MIF and TGF-β levels, and the signalling mediated by these cytokines was similar in both these groups. IFN-II, TNF, and complement-mediated signalling are known to be

activated in response to Mtb infection. The complement pathway mediates the uptake of Mtb by mononuclear phagocytes; the IFN-II pathway coordinates and maintains mononuclear inflammation, while the TNF pathway is responsible for initiating cytokine and chemokine responses. Exploring the outgoing signal pattern showed that Th1 cells and CD4+ CTLs were majorly responsible for IFN-II mediated signalling in the TB group with some contribution from NK CD160+ cells, CD8+ effector and naïve CD8+ T cells (Figure 6E). For TNF-mediated signalling, alveolar macrophages, CD4+ CTLs and Th17 cells were major contributors in the TB group (Supplementary Figure S12). CellChat circle plots showed a significantly reduced TNF and IFN-II signalling strength in the DM-TB compared to the TB group (Figure 6E, Supplementary Figure S12). Reduced IFN-II, TNF, and complement signalling, and increased IL-6 and IL-16 communication in the DM-TB group, indicate a skewed inflammatory response in this group, which could be detrimental to the host.

Chronic TB infection in DM condition leads to increased bacterial burden: To investigate the consequences of long-term chronic TB infection in DM mice, we repeated the entire experiment with an additional 8 w.p.i. time point (Figure 7A). In a recent study, Martinez et al. showed that diabetic mice developed using a high-fat diet (HFD) model showed significantly increased lung CFU at 8 w.p.i. with Mtb Erdman.[10] In the current study, NA-STZ induced T2DM and control C57BL/6 male mice were aerosol infected with 100-120 CFU of Mtb H37RV. NA-STZ induced diabetic mice showed an expected reduction in body weight upon STZ induction with consistent hyperglycemia over the 110 days of the study period (Figure 7B, 7C). At 3 w.p.i., we did not observe a significant lung or spleen weight increase between study groups (Figure 7D). The lung mycobacterial burden at 3 w.p.i. was comparable between TB and DM-TB groups, replicating earlier experimental findings (Figure 7E). However, at 8 w.p.i., we observed mild splenomegaly and a significant increase in the lung weight of DM-TB mice, which indicates a hyper-inflammatory state (Figure 7F), also evident in H&E-stained lung tissue sections for this group (Figure 7H, 7I). Upon chronic infection, at 8 w.p.i., an increased lung mycobacterial load in DM-TB mice was observed, corroborating earlier reports (Figure 7G).[8,10]

Discussion

Hyperglycemia is a characteristic feature of T2DM and has been associated with microvascular and macrovascular complications such as atherosclerosis, retinopathy, nephropathy and neuropathy.[45-48] Diabetes also renders the host susceptible to several pathogenic attacks like COVID-19, candida, influenza, Mtb and *Helicobacter pylori*.[15,48,49] This increased susceptibility to infections is owed to disrupted immune responses in diabetic conditions, such as impaired immune cell functions like chemotaxis, reduced phagocytic ability and insufficient cytokine response.[15,48,49]

To understand the effect of diabetes on lung immune dynamics, the STZ-NA model of diabetes induction, which mimics human complications of T2DM, was followed.[9] While genetic and diet-based models of T2DM are widely used in research, these mice take longer duration to develop hyperglycemia.[10] NA-STZ induced mice develop hyperglycemia 72 hours after the last dose, and most of the mice remain consistently hyperglycemic with T2DM associated complications. In addition, both genetic and diet-based models of diabetes lead to obesity, which contributes significantly towards organ

dysfunction and systemic inflammation. We aimed to understand the effects of hyperglycemia on host metabolism and immune dysfunction in the absence of confounding factors contributed by obesity. The DM induction method adopted in this study was a modified version of NA-STZ T2DM induction reported earlier.[9] Since Cheekatla et al. reported resistance to DM development in female mice, in this study, male mice were used with a reduced STZ dose of 150 mg/kg. Male C57BL/6 and BALB/c mice are reported to have a higher susceptibility to H37Rv infection with increased morbidity and mortality; thus, male mice were used in this study.[50] Post NA-STZ induction, mice's body weight and blood glucose were followed for a month to ascertain persistent hyperglycemia in the induced animals. We report that these mice show significant insulin resistance, glucose intolerance and dyslipidemia compared to euglycemic controls. While Cheekatla et al. reported these complications in their model, it took six months for female C57BL/6 mice to exhibit the metabolic disruptions. In contrast, male C57BL/6 mice adopted in this study developed complications within a month of hyperglycemia.[9] As discussed earlier, males are more susceptible to T2DM, and the early onset of disease severity in male C57BL/6 mice could be attributed to gender-associated differences.

Upon Mtb low dose (100-120 CFU) aerosol infection, the DM-TB and TB groups showed similar tissue mycobacterial burden at 3 w.p.i., corroborating earlier reports.[9] The gross tissue pathology and the spleen weight were similar between the DM-TB and TB groups. Upon histopathology analysis, it was evident that lung tissue from both groups had cellular infiltration. At 3 w.p.i., we did not observe any granulomatous structure in either group. However, upon chronic infection, i.e., 8 w.p.i., we observed an increased lung mycobacterial burden with significantly increased lung weight, indicating hyperinflammation in the lungs of DM-TB mice.

We observed a significantly perturbed serum cytokine profile in diabetic and DM-TB conditions, corroborating earlier reports.[17] Upon Mtb infection, there was a significant increase in circulatory IFN-γ in both hyperglycemic (DM-TB) and euglycemic (TB) groups compared to the uninfected controls. However, the heightened serum IFN-γ levels in the DM-TB group were comparatively lower than TB controls, indicating a dampened IFN-γ mediated anti-TB response. In addition, we observed significantly higher circulatory TNF-α levels in DM, TB and DM-TB groups compared to the healthy controls. Observed highest circulatory TNF-α levels in the DM-TB group could be due to infection-mediated augmentation of TNF-α levels to the already high circulatory TNF-α as a consequence of DM. While TNF-α is required by the host to combat Mtb infection, excess of it has been shown to increase susceptibility to the pathogen. Therefore, the increase in circulatory TNF-α levels due to cumulative effects of T2DM and TB could prove detrimental to the host due to higher susceptibility to pathogens and worsening insulin-resistant state.[19,20] IL-6 is associated with early-stage immune responses in Mtb infections and is responsible for accumulating lymphocytes and regulating mononuclear cell-driven inflammation.[51] However, increased baseline IL-6 levels in DM-TB conditions have been associated with worsened treatment outcomes. We observed significantly higher circulatory IL-6 levels in DM and DM-TB groups than in healthy controls. T2DM patients with higher IL-6 levels showed impaired insulin signalling via decreased activation of IRS-I and compromised liver glycogenesis.[52,53] In addition, we observed significantly increased circulatory IL-17A and TNF-α levels in DM and DM-TB groups,

corroborating earlier reports.[22] IL-17A increase can lead to excessive production of pro-inflammatory cytokines and chronic inflammation as it acts on NF-κB to upregulate the expression of pro-inflammatory cytokines.[22,54] A modest increase in circulatory IL-1β levels was observed in the DM-TB group compared to controls. Altogether, these data suggest a heightened baseline inflammatory state in DM-TB and DM groups with increased serum levels of pro-inflammatory cytokines like IL-6, TNF-α and IL-17A, which could be drivers of tissue pathology, worsened glycemic control and insulin resistance in NA-STZ induced DM and DM-TB mice.

The dissemination of Mtb precedes T-cell immunity.[23] Upon infection, Mtb enters host immune cells like macrophages and dendritic cells, which transport the bacteria to pulmonary lymph nodes (PLN). Here, T-cells are activated and migrate to the lungs.[23] Thus, macrophages, DCs and T-cells are the major immune cells involved in primary immune response to Mtb. Therefore, we sorted lung CD11C+ (macrophages and DCs) and CD3+ (T cells) cells at 21 days post-infection (3 w.p.i.) from the lungs of euglycemic (TB) and hyperglycemic groups (DM-TB, DM) and control mice (healthy). Reports show that diabetic (DM) mice delay T-cell migration to infection sites, thus compromising the anti-TB response in DM-TB comorbid conditions during the early stages of infection.[7] As expected, upon Mtb infection, the frequencies of CD11C+ and CD3+ cells were significantly higher in the lungs than in uninfected controls. However, the frequency of CD3+ cells was significantly lower in the DM-TB group lung cells than in TB. In contrast, CD11C+ cell frequency in the DM-TB group was lower than TB, although statistically insignificant. The reduced frequency of CD3+ cells in the lungs of DM-TB mice indicates a delay in T-cell migration to the site of infection, corroborating earlier reports.[7] An overall increase in the proportion of naïve CD4+ T-cells and Th17 cells in the DM group was observed. Increased frequency of Th17 cells has been associated with inflammageing, defined as chronic low-grade inflammation in the absence of infection accompanying ageing. T2DM has been associated with the early onset of inflammageing, even in the absence of obesity.[55] Reports show that aged individuals and T2DM patients present with increased Th17 frequencies.[56] Increased Th17 cell numbers are accompanied by higher circulatory IL-17A and IL-6 levels, and our findings corroborate earlier literature. IL-17 knockout mice models demonstrate improved insulin sensitivity, glucose tolerance and reduced pro-inflammatory cytokine levels.[22,56] Transplanting highly purified Th17 cells islet-reactive BDC2.5 TcR transgenic mice to non-obese diabetic (NOD) mice accelerated the onset of diabetes in these animals.[22] However, most of these studies have profiled circulatory immune cells, while we report that T2DM leads to increased Th17 cell number in the lungs of diabetic mice as well as low-grade chronic inflammation.

Genes involved in pyroptosis were significantly upregulated in naïve CD4+ T-cells from the lungs of DM mice compared to healthy controls. Pyroptosis is a gasdermin mediated cell death implicated in sterile inflammatory disorders such as T2DM, cancer, atherosclerosis and lung inflammation.[24] Inflammasome-mediated pyroptosis of pancreatic β-cells is well-known in T2DM.[24] In the current study, we observed that pyroptosis-mediated inflammation in T2DM is also prevalent in the lungs and not just limited to the pancreas. In our earlier work, we highlighted the multi-tissue metabolomic dysregulation in DM-TB conditions, and it might be interesting to see the multi-tissue immunological consequences of T2DM.[57] Th17 cells, intermediate monocytes and naïve CD8+ T cells, were also major drivers of

increased IL-16 signalling in the lungs of diabetic mice. In ova-induced mice models of asthma, IL-16 has been identified as a major driver of airway inflammation. Increased IL-16 signalling in immune cells from diabetic mice indicates increased baseline respiratory inflammation.[31] Histology analysis of lung tissue sections from 3 and 8 w.p.i. mice exhibited increased tissue inflammation in DM-TB conditions, where the increased IL-16 signalling could be the major driver and needs further exploration.

Naïve CD4+ T-cells and Th17 cells were higher in the lungs of DM-TB mice than in TB, while the number of M1 macrophages, Th1 cells and CD4+ CTLs were lower. Th1 cells are IFN-γ secreting cells that activate macrophages to mediate Mtb killing and also play an anti-inflammatory role by restricting tissue-damaging IL-17 responses.[58] Increased CD4+ CTLs presence in the circulation of drug-sensitive active TB patients was reported recently.[59] CD4+ CTLs have been studied extensively in viral infections such as dengue, influenza, hepatitis and HIV, where these cells exert cytotoxic and protective roles.[60] CD4+ CTLs, like Th1 cells, are IFN-γ secreting cells and might be involved in anti-TB activity by activating macrophages. In addition, these cells act majorly via MHC-II interactions and, therefore, might be involved in the killing of Mtb harbouring macrophages in the host lungs via the secretion of cytolytic molecules such as granzyme.[60] Literature exploring the role of CD4 CTLs in the context of bacterial infections, specifically Mtb, is scarce, and further detailed studies are needed to understand the role of these cells upon Mtb infection. M1 macrophages play a crucial role in pro-inflammatory host responses against intracellular bacteria. These cells exhibit high expression of iNOS, leading to NO production, which is detrimental to intracellular bacteria, such as Mtb.[61,62] In addition, M1 macrophages, polarised by IFN-γ, secrete pro-inflammatory cytokines, anti-microbial peptides and proteolytic enzymes.[61,62] Mtb blocks M1 polarisation by restricting the expression of IFN-γ responsive genes by inducing secretion of IL-6.[21] Mtb ESAT-6 also limits NF-κB2 and IFN-γ regulatory factors downstream of TLR2 signalling. SCENIC analysis showed significant downregulation of NF-κB2 in M1 and alveolar macrophages from the DM-TB group compared to TB controls. CellChat analysis identified a reduced MIF signalling pathway in M1 Mϕ from DM-TB mice compared to the TB group. It is worth noting that both TL2 signalling and MIF signalling are regulated via NF-κB2, and this regulatory factor's compromised activation points towards a disrupted M1 functionality in DM-TB condition. The reduced proportions of Th1, M1 Mϕ and CD4+CTLs in the lung of DM-TB mice indicate an impaired anti-TB immune response in this group.

In the current study, we have attempted to elucidate the lung immune landscape of DM-TB comorbid conditions. However, the current study has a few limitations. Gender-based differences are reported in the context of metabolic as well as immunological consequences of DM-TB comorbidity. In this study, male C57BL/6 mice were used for the immunological studies. Expanding this work to female mice would greatly enrich the insights gathered from the current work. In the current study, we have used chemical diabetes induction methods. A study employing alternate DM models such as HFD-induced or genetic models (Akita mice, db/db mice) would help us understand whether similar immunological consequences of DM are observed across models. In addition, the effect of anti-diabetic drugs such as insulin, GLP inhibitors or metformin on immunological consequences of DM-TB comorbid condition remains to be explored. In addition, we have observed the deregulation of several cytokines in DM

conditions, such as MIF, IL-16 and TGF-β, all of which play a crucial role in host TB defence. Therefore, in-vivo inhibition of these inflammatory cytokines in a model system using monoclonal antibodies might reduce disease severity in DM-TB comorbidity and needs further exploration.

However, findings of this study show that DM-TB comorbid conditions result in disrupted immunological host profiles compared to euglycemic control. A dampened immune response to Mtb might increase the disease severity in comorbid individuals. This work provides a rich baseline data set and provides cellular and molecular details as a resource to enhance our understanding of the DM-TB comorbid condition, and subsequent validation studies involving human subjects would be instrumental in designing targeted drug interventions.

STAR ★ Methods

Diabetes induction: The animal experimental protocols followed in this study are approved by the animal ethics committee (vide reference ICGEB/IAEC/07032020/TH-13Ext) of the International Centre for Genetic Engineering and Biotechnology New Delhi component. As reported earlier, DM was induced in male C57BL/6 mice of 8-12 weeks of age by combined administration of STZ and NA, with minor modifications.[9] Mice were fasted for 16 hours before NA and STZ administration. NA (60 mg/kg in 0.9% saline) was administered intraperitoneally 15 minutes before STZ injection. STZ (150 mg/kg in 50mM citric acid buffer) was administered intraperitoneally thrice with an interval of 10 days between doses. Age and gender matched control mice received intraperitoneal injections of the corresponding vehicle solution. Mice with fasting plasma glucose >200 mg/dL (measured using Dr. Morepen Gluco-One BG-03 glucometer) were grouped as diabetic (DM). Body weight and 6 hours of fasting blood glucose were monitored weekly till experiment completion.

Intra peritoneal Glucose tolerance test (iPGTT) and Insulin Tolerance Test (ITT): Mice were fasted for 6 hours with access to drinking water at all times. For iPGTT, mice were weighed and intra-peritoneally injected with a 20% glucose solution (2g of glucose/kg body mass). For ITT, mice were weighed, and the volume of 0.25 UI insulin solution required for IP injection was calculated using the formula: volume of IP insulin injection (µl) = 3 x body weight (g). The baseline glucose level (t = 0) was measured using the Dr. Morepen Gluco-One BG-03 glucometer. Mice were injected intraperitoneally with the appropriate amount of glucose solution, as previously determined, and the time-point of injection was recorded. Blood glucose levels were measured 15, 30, 60, 90 and 120 minutes after glucose injection by placing a small drop of blood on a new test strip and recording the measurements. At the end of the experimental session, water and food were provided ad libitum.

Mtb H37Rv infection: After 60 days of consistent hyperglycemia, C57Bl/6 mice were infected with a low aerosol dose (100-120 CFU/animal) of animal passaged Mtb H37Rv using a Madison chamber in a tuberculosis aerosol challenge BSL-III facility at the host institution. Before infection, Mtb H37Rv was grown to log phase in 7H9 medium supplemented with OADC (10%, Difco Middlebrook). The PDIM levels of the Mtb H37Rv strain were monitored using standard procedure. For infection, bacterial culture (1 ml) was washed with Phosphate Buffer Saline (PBS, pH 7.4, 9 ml) and centrifuged at 4,000 g for 10 minutes at room temperature. After discarding the supernatant, the resulting pellet was resuspended

using PBS (1 ml). The bacterial single-cell suspension was prepared in PBS (15 ml) and adjusted to 1 × 10^6 cells/ml before loading to the nebuliser chamber for infection. Study mice were exposed to aerosol for 20 minutes in a Madison chamber, which delivers 100-120 Colony-forming units (CFU)/animal. After 1-, 21- and 56 days post-infection (d.p.i.; 3- and 8-weeks post infection), animals were anaesthetized for whole blood collection via retro-orbital puncture and serum samples were isolated. At 21 and 56 d.p.i., organs (lung, liver and spleen) were harvested for bacterial CFU assay, histology and immune cell isolation. Part of the lungs was stored in buffered formalin solution for histology analysis using standard hematoxylin and eosin staining methods. For CFU enumeration, the spleen, lung and liver were homogenized in phosphate buffer saline (PBS) and plated on 7H11 media supplemented with OADC (10%), BBL MGIT PANTA and thiophene carboxylic acid hydrazide (TCH; 20 µg/ml) in triplicates and CFU counting was carried out 21 days later.

Serum insulin, fatty acids, cholesterol and triglyceride measurements: Mice were anaesthetized using isoflurane and whole blood was collected via retro-orbital puncture for all study animals. Whole blood was allowed to clot at room temperature for 20 minutes and then centrifuged at 2,000 rpm at 4°C for 10 minutes. Serum was transferred to a fresh micro-centrifuge tube and stored at -80°C until further processing. Random serum insulin levels of all mice groups were measured using a Rat / Mouse Insulin ELISA Kit (#EZRMI-13K, Merck Millipore, USA) following the manufacturer's instructions. Serum-free fatty acids (#700310), cholesterol (#10007640), and triglyceride (#10010303) levels were measured using either a fluorometric or colourimetric assay (Cayman Chemicals, USA), following the manufacturer's instructions.

Cytokine measurement and analysis using LEGENDplex™: Test serum samples were thawed on ice and centrifuged at 2,000 rpm for 5 minutes at 4°C. Wash buffer, matrix C and standards were prepared per the manufacturer's instructions. Serum samples (25 µl) were diluted 2-fold with assay buffer, and cytokine (IFN-γ, Il-6, TNF-α, IL-17A, IL-23, IL-1α and IL-1β) estimation was performed as per manufacturer's instructions (BioLegend, California, USA).

Lung immune cell isolation: Lungs of study groups were chopped into smaller pieces using surgical scissors and digested at 37°C and 180 rpm for 30 minutes in RPMI (Gibco, 31800022) containing collagenase D (2 µg/µl, Sigma-Aldrich Chemicals Pvt Limited, 101088866001) and DNase-I (1 µg/µl, Sigma-Aldrich Chemicals Pvt Limited, 10104159001). Following incubation, samples were passed through a 70 µm nylon mesh cell strainer, and the single-cell suspension was collected in a 15 ml centrifuge tube. Samples were centrifuged at 250 g at 4°C for 5 min, and the resulting cell pellet was resuspended in ACK lysis solution (1 ml). Samples were incubated for 3 min at room temperature, and lysis was stopped by adding ice-cold 10% FACS buffer (2 ml) to each sample. Samples were centrifuged at 250 g at 4°C for 5 min, and the pellet was resuspended in 1 mL of 10% FACS buffer. Cells were enumerated using Countess 3 (Thermo Fisher Scientific, USA), and viability was determined by trypan blue staining.

Cell surface protein staining and FACS sorting: After transferring the cells to a new 2-ml microcentrifuge tube, it was centrifuged at 250 × g at 4°C for 5 min. The pellet was resuspended in 94

µl chilled PBS supplemented with FBS (10%). TruStain FcX (0.5 µl) and True-Stain Monocyte Blocker (5 µl) were added to the cells and incubated for 10 min at 4°C. To respective samples, BioLegend TotalSeq™-B hashtags (0.5 µl) were added and incubated for 30 min at 4°C. Samples were diluted with PBS supplemented with FBS (10%), and after making the final volume to 2 ml were centrifuged at 250 × g at 4°C for 5 min. The pellet was resuspended in diluted live/dead stain (98.5 µl) and FACS antibody mix and incubated for 45 min at 4°C without light exposure. Samples, after diluting in PBS supplemented with FBS (10%) were made to the final volume of 2 ml and centrifuged at 250 g at 4°C for 5 min. The pellet was resuspended in 1.5 ml of chilled PBS supplemented with FBS (10%) and transferred to 5 ml round-bottom polystyrene tubes and flow sorted cells were collected in 1 ml chilled PBS supplemented with FBS (50%).

Sample Fixation for scRNAseq: Flow sorted cells were counted using Countess 3 (Thermofisher Scientific, USA). CD3+ and CD11C+ cells were mixed in a ratio of 2:1 in a 15 ml centrifuge tube and centrifuged at 250 g at 4°C for 5 min. The supernatant was discarded, and cells were fixed, following the manufacturer's protocol. Briefly, cells were resuspended in room temperature fixation buffer (1 ml, 10x Genomics PN-2000517) and incubated at 4°C for 24 hours. Samples were then centrifuged at 250 g at 4°C for 5 min, resuspended in quenching solution (1 ml, 10x Genomics, USA PN-2000516) and transferred to a 2 ml DNA LoBind (022431048, Eppendorf) tube. Enhancer (10x Genomics, PN-2000482) was thawed and pre-warmed at 65°C for 10 minutes. Glycerol (50%, 275 µl, G5516, Millipore Sigma) and enhancer (100 µl) were added to the quenched cells and samples were stored at -80°C until further processing.

Fixed single-cell RNA gene expression profiling: The fixed cells stored at -80°C were used for fixed single-cell RNA sequencing 10x Genomics single-cell gene expression flex kit. Probe hybridization, GEM generation, barcoding and library construction were performed following manufacturer's instructions. Sample libraries were stored at -20°C until sequencing, and an aliquot (1 µl) was used for library QC using D1000 ScreenTape with Agilent TapeStation (Agilent Technologies, USA). Gene expression (GEX) and cell surface protein (CSP) libraries were sequenced using PE150 chemistry on an SP100 flow cell in a third-party NovaSeq 6000 sequencing system (Illumina, USA). The sequencing depth was 10,000 read pairs/cell for GEX libraries and 5,000 read pairs/cell for CSP libraries. A 10% PhiX spike was used while loading for the sequencing of these libraries.

scRNAseq data analysis: All the scRNA-seq raw and processed data files are accessible from Gene Expression Omnibus (GEO) database with accession number GSE280089. FASTQ files obtained from the NovaSeq6000 sequencing system were run through Cell Ranger (v7.2) multi pipeline. After successfully running the Cell Ranger multi pipeline, the output folder "filtered_feature_bc_matrix" generated for each sample was used for further data analysis using the Seurat V5 package in R. The scRNA seq data analysis was divided majorly into Mtb infected and uninfected control groups. Samples were read using the Read10X function of Seurat. Data was subsetted using the following filter parameters: nFeature_RNA (no. of features/cell) = 1000-7000, nCount_RNA (UMI count/cell) =1500-20000 and percent.mt (mitochondrial RNA percentage) ≤ 5. Data was normalised using the

NormalizeData function of the Seurat package, where the count data in RNA assay is log normalised, and a scale factor of 10,000 is used for cell-level normalisation. FindVariableFeatures function was used to identify features in the dataset that were classified as outliers on a 'mean variability plot'. VST (variance stabilising transformation) was used as a selection method, accounting for the variance-mean gene expression relationship with a regression model. For comparative analysis of two different datasets, the Seurat object for each dataset needs to be integrated. Before integrating Seurat objects, the FindIntegrationAnchors function is used to find a set of anchors between a list of Seurat objects. These anchors are then used to integrate the objects using the IntegrateData function. A list of genes to keep in the merged object post-integration was defined to ensure that genes are not subsetted into different layers of the Seurat object post-integration. Then, the IntegrateData function was used to perform dataset integration. features.to.integrate into the IntegrateData was defined as the list of genes prepared in the previous step. DefaultAssay was set to the “integrated” layer of the merged Seurat object for further data analysis. The features in the dataset were scaled and centered using the ScaleData function, where the maximum value to return for scaled data was set at 10. Dimensionality reduction in the dataset was performed using the RunUMAP function, which runs the Uniform Manifold Approximation and Projection (UMAP) dimensionality reduction technique. FindNeighbors function was used to compute the k.param nearest neighbours for the integrated dataset. FindClusters function was used to identify cell clusters by a shared nearest neighbour (SNN) modularity optimization-based clustering algorithm. The custom function was used to plot integrated clusters as bar plots with cluster identity on the X-axis and the number of cells per cluster on the Y-axis. ScType package was used for cluster annotation, a cell-type identification algorithm that uses a comprehensive cell marker database as background information to assign an identity to a cell. The datasets were subsetted into myeloid (Itgam+ Itgax+ Cd13+ Cd14+), and lymphoid (Cd3e+ Cd4+ Cd8a+ Cd8b+) clusters based on canonical marker expression and reclustered to identify further sub-clusters in these cell populations.

Differential gene expression (DGE) analysis: DESeq2 package was used for differential expression analysis to identify differences in the gene expression between study groups. Before proceeding with DESeq2 analysis, the scRNA seq samples must be pseudobulked. A pseudobulk sample is formed by aggregating the expression values for a group of cells from the biological replicate. Since we used cell surface protein labels for multiplexing four biological replicates for each study group, we fetched the antibody data from cell ranger output and assigned a replicate identity to each cell and the group identity. This was done using custom functions and resulted in merging the replicate information to the metadata of the Seurat object. AggregateExpression function from the Seurat package was then used to pseudobulk data, which returns summed counts for each study group. DGE analysis was performed using the DESeq2 package, which estimates dispersion and fits a negative binomial model to the count data. During analysis, euglycemic control (TB or healthy) groups were set as reference levels to use as a baseline for comparison. DGE analysis was performed for individual cell clusters between study groups to identify diabetes-associated changes in gene expression for each cell type.

CellChat analysis: CellChat is an R package that uses gene expression data of a cell and models the probability of cell-cell communication.[63] This package integrates gene expression with the CellChat

database, which details interactions between signalling ligands, receptors and their cofactors. CellChat analysis used cell annotation to identify the study group, and cell-cell communication was computed for each study group independently. CellChatDB.mouse was a database comprising a list of ligand-receptor interactions in the mice. Cell-cell communication probability was computed between interacting cell clusters using the computeCommunProb function with trimean to compute average gene expression per cell group. computeCommunProbPathway function was used to calculate communication probability for a signalling pathway by summarising all related ligands/receptors, and the aggregateNet function was used to calculate aggregated cell-cell communication. Each study group's resulting CellChat object was exported as a .rds file. The cellchat .rds file for each study group was imported for comparative CellChat analysis, and network centrality was computed using the netAnalysis_computeCentrality function for each sample. The CellChat objects for each study group were merged using the mergeCellChat function. Using the compareInteractions function, the total number of interactions and strength was compared between datasets to assess whether cell-cell communication was altered between groups. netVisual_diffInteraction function was used to differential cell-cell communication between study groups. The ranked function compared the information flow between groups' signalling pathways.

SCENIC analysis: The Single-Cell Regulatory Network Inference and Clustering (SCENIC) package allows differential activation states of transcription factors and gene regulatory networks in cell types from scRNA-seq data.[64] SCENIC analysis was done using Python. Outputs from the SCENIC analysis were exported as .loom files. QC-filtered Seurat objects for each dataset were exported as .rds files, and .loom files were prepared from .rds objects and used for SCENIC analysis. Gene regulatory inference was performed using the GRNBoost2 algorithm. This step identifies potential targets for each transcription factor based on co-expression. Next, regulon prediction was performed based on DNA motif analysis. For this, ranking and motif annotations databases for mice were downloaded from the cisTarget resources website. Network activity in individual cells was analysed using AUCell, which allows the identification of cells with active gene sets. The resulting files were used in R for comparative regulon analysis between groups. Integrated .rds object and .csv file containing auc information were imported for study groups, and the unpaired Wilcoxon rank-sum test was performed on each common regulon from study groups to identify significantly deregulated regulons. Combinations with p-value ≤ 0.05 were defined as significant differential regulons and used to plot data as a cluster map.

Statistical Analysis: Animal body weight, blood glucose, Mtb H37Rv CFU, iPGTT, ITT, cytokine concentration and immune cell frequency data were analysed by parametric analysis using Student's t-test and area under curve (AUC) analysis in GraphPad Prism (version 8.4.2, GraphPad Software, San Diego, CA). R packages pheatmap, Dimplot, Nebulosa, DotPlot, ggplot2, EnhancedVolcano, ComplexHeatmap, Rcolorbrewer, scCustomize, vlnplot and corrplot were used to generate plots. FlowJo (version 10.7.1, BD Biosciences, Ashland, USA) was used for FACS data analysis. LEGENDplex data was analysed using BioLegend's LEGENDplex™ data analysis software (Version 2024-06-15, LEGENDplex Qognit).

Acknowledgement: SC is a Shyama Prasad Mukherjee fellow and was supported by the Council of Scientific and Industrial Research, Government of India. A fellowship from the Department of Biotechnology, Government of India, supported MS and FP. The core support from the International Centre for Genetic Engineering and Biotechnology (ICGEB), New Delhi, to RKN; core support from the National Institute of Immunology, New Delhi, to DM; core support from the Institute of Life Sciences Bhubaneswar to DD are highly acknowledged. Nidhi Yadav and Ashish Gupta are acknowledged for their help and support during the animal experiments. Help from the staff of the bio-experimentation facility and Tuberculosis Aerosol Challenge Facility (TACF) at ICGEB, New Delhi, is acknowledged. TACF is supported by the Department of Biotechnology, Government of India. We thank Dr. Veena Patil and Mr. Raunak Kar from the National Institute of Immunology, New Delhi, for their help with the single-cell RNA sequencing experiments. For the SCENIC analysis, CSIR-IGIB Tejas HPC compute is acknowledged. Part of these research findings was presented as a poster at the Global Immunology Summit 2024 at THSTI on 22nd February 2024. Some figures have been created with Biorender.com.

Author Contribution: S. C. and R. N. conceptualization, S. C., M. S., F. P. and R. N. methodology, S. C. visualization, S. C., P.S. and S.V. formal analysis, S. C. and R. N. writing–original draft; S. C., D. M., D. D., R. N. review – final draft, D. M., D. D. and R. N. supervision.

Conflict of interest: The authors declare that they have no known competing financial interests or personal relationships that could have appeared to influence the work reported in this paper.

References:

1. Bagcchi, S. (2023). WHO's Global Tuberculosis Report 2022. Lancet Microbe *4*, e20. 10.1016/S2666-5247(22)00359-7.
2. Pai, M., Behr, M.A., Dowdy, D., Dheda, K., Divangahi, M., Boehme, C.C., Ginsberg, A., Swaminathan, S., Spigelman, M., Getahun, H., Menzies, D., and Raviglione, M. (2016). Tuberculosis. Nat Rev Dis Primers *2*, 16076. 10.1038/nrdp.2016.76.
3. Magliano, D.J., and Boyko, E.J. (2021). In IDF DIABETES ATLAS.
4. Dooley, K.E., and Chaisson, R.E. (2009). Tuberculosis and diabetes mellitus: convergence of two epidemics. Lancet Infect Dis *9*, 737-746. 10.1016/S1473-3099(09)70282-8.
5. Kumar Nathella, P., and Babu, S. (2017). Influence of diabetes mellitus on immunity to human tuberculosis. Immunology *152*, 13-24. 10.1111/imm.12762.
6. Gupte, A.N., Kumar, P., Araujo-Pereira, M., Kulkarni, V., Paradkar, M., Pradhan, N., Menon, P., Padmapriyadarsini, C., Hanna, L.E., Yogendra Shivakumar, S.V.B., et al. (2022). Baseline IL-6 is a biomarker for unfavourable tuberculosis treatment outcomes: a multisite discovery and validation study. Eur Respir J *59*. 10.1183/13993003.00905-2021.
7. Vallerskog, T., Martens, G.W., and Kornfeld, H. (2010). Diabetic mice display a delayed adaptive immune response to Mycobacterium tuberculosis. J Immunol *184*, 6275-6282. 10.4049/jimmunol.1000304.
8. Martinez, N., and Kornfeld, H. (2014). Diabetes and immunity to tuberculosis. Eur J Immunol *44*, 617-626. 10.1002/eji.201344301.
9. Cheekatla, S.S., Tripathi, D., Venkatasubramanian, S., Nathella, P.K., Paidipally, P., Ishibashi, M., Welch, E., Tvinnereim, A.R., Ikebe, M., Valluri, V.L., et al. (2016). NK-CD11c+ Cell Crosstalk in Diabetes Enhances IL-6-Mediated Inflammation during Mycobacterium tuberculosis Infection. PLoS Pathog *12*, e1005972. 10.1371/journal.ppat.1005972.
10. Martinez, N., Smulan, L.J., Jameson, M.L., Smith, C.M., Cavallo, K., Bellerose, M., Williams, J., West, K., Sassetti, C.M., Singhal, A., and Kornfeld, H. (2023). Glycerol contributes to tuberculosis susceptibility in male mice with type 2 diabetes. Nat Commun *14*, 5840. 10.1038/s41467-023-41519-9.
11. Gideon, H.P., Hughes, T.K., Tzouanas, C.N., Wadsworth, M.H., 2nd, Tu, A.A., Gierahn, T.M., Peters, J.M., Hopkins, F.F., Wei, J.R., Kummerlowe, C., et al. (2022). Multimodal profiling of lung granulomas in macaques reveals cellular correlates of tuberculosis control. Immunity *55*, 827-846 e810. 10.1016/j.immuni.2022.04.004.
12. Bromley, J.D., Ganchua, S.K.C., Nyquist, S.K., Maiello, P., Chao, M., Borish, H.J., Rodgers, M., Tomko, J., Kracinovsky, K., Mugahid, D., et al. (2024). CD4(+) T cells re-wire granuloma cellularity and regulatory networks to promote immunomodulation following Mtb reinfection. Immunity *57*, 2380-2398 e2386. 10.1016/j.immuni.2024.08.002.
13. Akter, S., Chauhan, K.S., Dunlap, M.D., Choreno-Parra, J.A., Lu, L., Esaulova, E., Zuniga, J., Artyomov, M.N., Kaushal, D., and Khader, S.A. (2022). Mycobacterium tuberculosis infection drives a type I IFN signature in lung lymphocytes. Cell Rep *39*, 110983. 10.1016/j.celrep.2022.110983.

14. Das, S., Marin, N.D., Esaulova, E., Ahmed, M., Swain, A., Rosa, B.A., Mitreva, M., Rangel-Moreno, J., Netea, M.G., Barreiro, L.B., et al. (2021). Lung Epithelial Signaling Mediates Early Vaccine-Induced CD4(+) T Cell Activation and Mycobacterium tuberculosis Control. mBio *12*, e0146821. 10.1128/mBio.01468-21.
15. Daryabor, G., Atashzar, M.R., Kabelitz, D., Meri, S., and Kalantar, K. (2020). The Effects of Type 2 Diabetes Mellitus on Organ Metabolism and the Immune System. Front Immunol *11*, 1582. 10.3389/fimmu.2020.01582.
16. Shanmuganathan, G., Orujyan, D., Narinyan, W., Poladian, N., Dhama, S., Parthasarathy, A., Ha, A., Tran, D., Velpuri, P., Nguyen, K.H., and Venketaraman, V. (2022). Role of Interferons in Mycobacterium tuberculosis Infection. Clin Pract *12*, 788-796. 10.3390/clinpract12050082.
17. Domingo-Gonzalez, R., Prince, O., Cooper, A., and Khader, S.A. (2016). Cytokines and Chemokines in Mycobacterium tuberculosis Infection. Microbiol Spectr *4*. 10.1128/microbiolspec.TBTB2-0018-2016.
18. Robert, M., and Miossec, P. (2021). Reactivation of latent tuberculosis with TNF inhibitors: critical role of the beta 2 chain of the IL-12 receptor. Cell Mol Immunol *18*, 1644-1651. 10.1038/s41423-021-00694-9.
19. Roca, F.J., Whitworth, L.J., Prag, H.A., Murphy, M.P., and Ramakrishnan, L. (2022). Tumor necrosis factor induces pathogenic mitochondrial ROS in tuberculosis through reverse electron transport. Science *376*, eabh2841. 10.1126/science.abh2841.
20. Stephens, J.M., Lee, J., and Pilch, P.F. (1997). Tumor necrosis factor-alpha-induced insulin resistance in 3T3-L1 adipocytes is accompanied by a loss of insulin receptor substrate-1 and GLUT4 expression without a loss of insulin receptor-mediated signal transduction. J Biol Chem *272*, 971-976. 10.1074/jbc.272.2.971.
21. Boni, F.G., Hamdi, I., Koundi, L.M., Shrestha, K., and Xie, J. (2022). Cytokine storm in tuberculosis and IL-6 involvement. Infect Genet Evol *97*, 105166. 10.1016/j.meegid.2021.105166.
22. Abdel-Moneim, A., Bakery, H.H., and Allam, G. (2018). The potential pathogenic role of IL-17/Th17 cells in both type 1 and type 2 diabetes mellitus. Biomed Pharmacother *101*, 287-292. 10.1016/j.biopha.2018.02.103.
23. Chackerian, A.A., Alt, J.M., Perera, T.V., Dascher, C.C., and Behar, S.M. (2002). Dissemination of Mycobacterium tuberculosis is influenced by host factors and precedes the initiation of T-cell immunity. Infect Immun *70*, 4501-4509. 10.1128/IAI.70.8.4501-4509.2002.
24. Li, T., Zheng, G., Li, B., and Tang, L. (2021). Pyroptosis: A promising therapeutic target for noninfectious diseases. Cell Prolif *54*, e13137. 10.1111/cpr.13137.
25. Mayer-Barber, K.D., and Yan, B. (2017). Clash of the Cytokine Titans: counter-regulation of interleukin-1 and type I interferon-mediated inflammatory responses. Cell Mol Immunol *14*, 22-35. 10.1038/cmi.2016.25.
26. Cao, Z., Sun, X., Icli, B., Wara, A.K., and Feinberg, M.W. (2010). Role of Kruppel-like factors in leukocyte development, function, and disease. Blood *116*, 4404-4414. 10.1182/blood-2010-05-285353.

27. Guo, J., Xue, Z., Ma, R., Yi, W., Hui, Z., Guo, Y., Yao, Y., Cao, W., Wang, J., Ju, Z., Lu, L., and Wang, L. (2020). The transcription factor Zfp281 sustains CD4(+) T lymphocyte activation through directly repressing Ctla-4 transcription. Cell Mol Immunol *17*, 1222-1232. 10.1038/s41423-019-0289-y.
28. Delpoux, A., Marcel, N., Hess Michelini, R., Katayama, C.D., Allison, K.A., Glass, C.K., Quinones-Parra, S.M., Murre, C., Loh, L., Kedzierska, K., et al. (2021). FOXO1 constrains activation and regulates senescence in CD8 T cells. Cell Rep *34*, 108674. 10.1016/j.celrep.2020.108674.
29. Calandra, T., and Roger, T. (2003). Macrophage migration inhibitory factor: a regulator of innate immunity. Nat Rev Immunol *3*, 791-800. 10.1038/nri1200.
30. Cytokine Reference, Two-Volume Set (Individual Version): A Compendium of Cytokines and Other Mediators of Host Defense. (2000). (Elsevier Science).
31. Li, C., Dai, J., Dong, G., Ma, Q., Li, Z., Zhang, H., Yan, F., Zhang, J., Wang, B., Shi, H., et al. (2019). Interleukin-16 aggravates ovalbumin-induced allergic inflammation by enhancing Th2 and Th17 cytokine production in a mouse model. Immunology *157*, 257-267. 10.1111/imm.13068.
32. Halvorsen, B., Santilli, F., Scholz, H., Sahraoui, A., Gulseth, H.L., Wium, C., Lattanzio, S., Formoso, G., Di Fulvio, P., Otterdal, K., et al. (2016). LIGHT/TNFSF14 is increased in patients with type 2 diabetes mellitus and promotes islet cell dysfunction and endothelial cell inflammation in vitro. Diabetologia *59*, 2134-2144. 10.1007/s00125-016-4036-y.
33. Kou, Y.B., Yan, X.Q., Jing, Q.Y., Zhang, S.H., Liu, Z.Z., Wei, Y.X., and Wang, Y.G. (2021). LIGHT (TNFSF14) inhibits glucose uptake of adipocytes by downregulating GLUT4 expression via AKT signaling pathway. Biochem Biophys Res Commun *583*, 106-113. 10.1016/j.bbrc.2021.10.061.
34. Xiao, M., Zhang, J., Chen, W., and Chen, W. (2018). M1-like tumor-associated macrophages activated by exosome-transferred THBS1 promote malignant migration in oral squamous cell carcinoma. J Exp Clin Cancer Res *37*, 143. 10.1186/s13046-018-0815-2.
35. Stein, E.V., Miller, T.W., Ivins-O'Keefe, K., Kaur, S., and Roberts, D.D. (2016). Secreted Thrombospondin-1 Regulates Macrophage Interleukin-1beta Production and Activation through CD47. Sci Rep *6*, 19684. 10.1038/srep19684.
36. Li, J., Wada, S., Weaver, L.K., Biswas, C., Behrens, E.M., and Arany, Z. (2019). Myeloid Folliculin balances mTOR activation to maintain innate immunity homeostasis. JCI Insight *5*. 10.1172/jci.insight.126939.
37. Porrello, A., Leslie, P.L., Harrison, E.B., Gorentla, B.K., Kattula, S., Ghosh, S.K., Azam, S.H., Holtzhausen, A., Chao, Y.L., Hayward, M.C., et al. (2018). Factor XIIIA-expressing inflammatory monocytes promote lung squamous cancer through fibrin cross-linking. Nat Commun *9*, 1988. 10.1038/s41467-018-04355-w.
38. Georgopoulos, K., Winandy, S., and Avitahl, N. (1997). The role of the Ikaros gene in lymphocyte development and homeostasis. Annu Rev Immunol *15*, 155-176. 10.1146/annurev.immunol.15.1.155.

39. Heizmann, B., Kastner, P., and Chan, S. (2018). The Ikaros family in lymphocyte development. Curr Opin Immunol *51*, 14-23. 10.1016/j.coi.2017.11.005.
40. Yordy, J.S., and Muise-Helmericks, R.C. (2000). Signal transduction and the Ets family of transcription factors. Oncogene *19*, 6503-6513. 10.1038/sj.onc.1204036.
41. Kaminskiy, Y., and Melenhorst, J.J. (2022). STAT3 Role in T-Cell Memory Formation. Int J Mol Sci *23*. 10.3390/ijms23052878.
42. Bonizzi, G., and Karin, M. (2004). The two NF-kappaB activation pathways and their role in innate and adaptive immunity. Trends Immunol *25*, 280-288. 10.1016/j.it.2004.03.008.
43. Sun, S.C. (2017). The non-canonical NF-kappaB pathway in immunity and inflammation. Nat Rev Immunol *17*, 545-558. 10.1038/nri.2017.52.
44. Su, H., Weng, S., Luo, L., Sun, Q., Lin, T., Ma, H., He, Y., Wu, J., Wang, H., Zhang, W., and Xu, Y. (2024). Mycobacterium tuberculosis hijacks host macrophages-derived interleukin 16 to block phagolysosome maturation for enhancing intracellular growth. Emerg Microbes Infect *13*, 2322663. 10.1080/22221751.2024.2322663.
45. E. Dale Abel, A.L.G., Carmella Evans-Molina, Joshua J. Joseph, Shivani Misra, Utpal B. Pajvani, Judith Simcox, Katalin Susztak, Daniel J. Drucker (2024). Diabetes mellitus—Progress and opportunities in the evolving epidemic. Cell *187*, 3789-3820. j.cell.2024.06.029.
46. Katsarou, A., Gudbjornsdottir, S., Rawshani, A., Dabelea, D., Bonifacio, E., Anderson, B.J., Jacobsen, L.M., Schatz, D.A., and Lernmark, A. (2017). Type 1 diabetes mellitus. Nat Rev Dis Primers *3*, 17016. 10.1038/nrdp.2017.16.
47. DeFronzo, R.A., Ferrannini, E., Groop, L., Henry, R.R., Herman, W.H., Holst, J.J., Hu, F.B., Kahn, C.R., Raz, I., Shulman, G.I., et al. (2015). Type 2 diabetes mellitus. Nat Rev Dis Primers *1*, 15019. 10.1038/nrdp.2015.19.
48. Papatheodorou, K., Banach, M., Bekiari, E., Rizzo, M., and Edmonds, M. (2018). Complications of Diabetes 2017. J Diabetes Res *2018*, 3086167. 10.1155/2018/3086167.
49. Berbudi, A., Rahmadika, N., Tjahjadi, A.I., and Ruslami, R. (2020). Type 2 Diabetes and its Impact on the Immune System. Curr Diabetes Rev *16*, 442-449. 10.2174/1573399815666191024085838.
50. Hertz, D., Dibbern, J., Eggers, L., von Borstel, L., and Schneider, B.E. (2020). Increased male susceptibility to Mycobacterium tuberculosis infection is associated with smaller B cell follicles in the lungs. Sci Rep *10*, 5142. 10.1038/s41598-020-61503-3.
51. Li, B., Jones, L.L., and Geiger, T.L. (2018). IL-6 Promotes T Cell Proliferation and Expansion under Inflammatory Conditions in Association with Low-Level RORgammat Expression. J Immunol *201*, 2934-2946. 10.4049/jimmunol.1800016.
52. Fasshauer, M., and Paschke, R. (2003). Regulation of adipocytokines and insulin resistance. Diabetologia *46*, 1594-1603. 10.1007/s00125-003-1228-z.
53. Kim, J.H., Kim, J.E., Liu, H.Y., Cao, W., and Chen, J. (2008). Regulation of interleukin-6-induced hepatic insulin resistance by mammalian target of rapamycin through the STAT3-SOCS3 pathway. J Biol Chem *283*, 708-715. 10.1074/jbc.M708568200.

54. Merino, K.M., Jazwinski, S.M., and Rout, N. (2021). Th17-type immunity and inflammation of aging. Aging (Albany NY) *13*, 13378-13379. 10.18632/aging.203119.
55. Prattichizzo, F., De Nigris, V., Spiga, R., Mancuso, E., La Sala, L., Antonicelli, R., Testa, R., Procopio, A.D., Olivieri, F., and Ceriello, A. (2018). Inflammageing and metaflammation: The yin and yang of type 2 diabetes. Ageing Res Rev *41*, 1-17. 10.1016/j.arr.2017.10.003.
56. Okamoto Yoshida, Y., Umemura, M., Yahagi, A., O'Brien, R.L., Ikuta, K., Kishihara, K., Hara, H., Nakae, S., Iwakura, Y., and Matsuzaki, G. (2010). Essential role of IL-17A in the formation of a mycobacterial infection-induced granuloma in the lung. J Immunol *184*, 4414-4422. 10.4049/jimmunol.0903332.
57. Chaudhary, S., Pahwa, F., and Nanda, R.K. (2024). Dysregulated cysteine metabolism leads to worsened liver pathology in diabetes-tuberculosis comorbid condition. J Biol Chem *300*, 105634. 10.1016/j.jbc.2024.105634.
58. Lyadova, I.V., and Panteleev, A.V. (2015). Th1 and Th17 Cells in Tuberculosis: Protection, Pathology, and Biomarkers. Mediators Inflamm *2015*, 854507. 10.1155/2015/854507.
59. Flores-Gonzalez, J., Ramon-Luing, L.A., Falfan-Valencia, R., Batista, C.V.F., Soto-Alvarez, S., Huerta-Nunez, L., and Chavez-Galan, L. (2024). The presence of cytotoxic CD4 and exhausted-like CD8+ T-cells is a signature of active tuberculosis. Biochim Biophys Acta Mol Basis Dis *1870*, 167219. 10.1016/j.bbadis.2024.167219.
60. Cenerenti, M., Saillard, M., Romero, P., and Jandus, C. (2022). The Era of Cytotoxic CD4 T Cells. Front Immunol *13*, 867189. 10.3389/fimmu.2022.867189.
61. Lugo-Villarino, G., Verollet, C., Maridonneau-Parini, I., and Neyrolles, O. (2011). Macrophage polarization: convergence point targeted by mycobacterium tuberculosis and HIV. Front Immunol *2*, 43. 10.3389/fimmu.2011.00043.
62. Khan, A., Zhang, K., Singh, V.K., Mishra, A., Kachroo, P., Bing, T., Won, J.H., Mani, A., Papanna, R., Mann, L.K., et al. (2022). Human M1 macrophages express unique innate immune response genes after mycobacterial infection to defend against tuberculosis. Commun Biol *5*, 480. 10.1038/s42003-022-03387-9.
63. Jin, S., Guerrero-Juarez, C.F., Zhang, L., Chang, I., Ramos, R., Kuan, C.H., Myung, P., Plikus, M.V., and Nie, Q. (2021). Inference and analysis of cell-cell communication using CellChat. Nat Commun *12*, 1088. 10.1038/s41467-021-21246-9.
64. Aibar, S., Gonzalez-Blas, C.B., Moerman, T., Huynh-Thu, V.A., Imrichova, H., Hulselmans, G., Rambow, F., Marine, J.C., Geurts, P., Aerts, J., et al. (2017). SCENIC: single-cell regulatory network inference and clustering. Nat Methods *14*, 1083-1086. 10.1038/nmeth.4463.

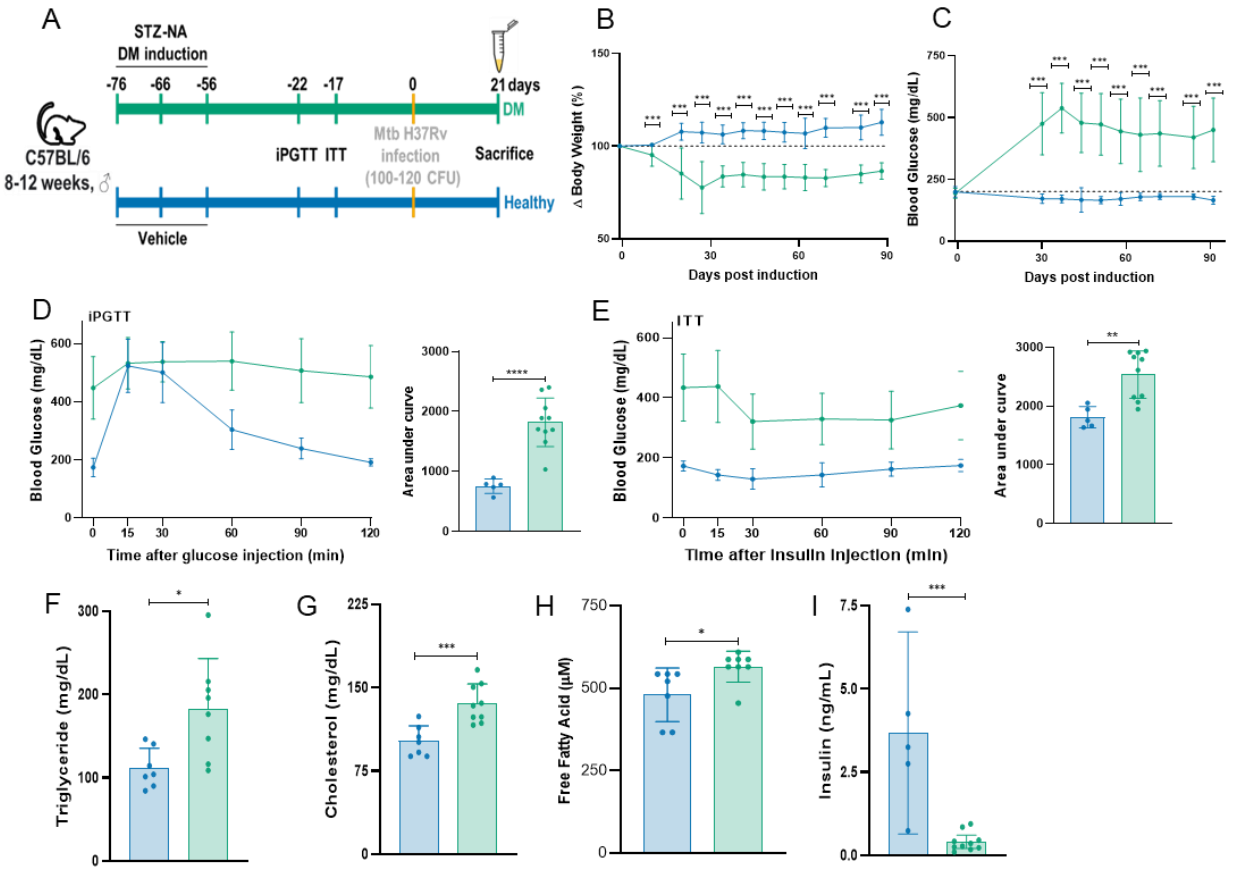

Figure 1: NA-STZ induced diabetes models Type 2 Diabetes Mellitus (DM) and its associated complications.

(A) Schematic representation of the experimental plan.

(B) Body weight change in DM and healthy mice during the course of the experiment. Healthy, n = 10; DM, n= 35. Error bars represent standard deviation.

(C) Fasting blood glucose in DM mice and healthy controls during the experiment. Healthy, n = 10; DM, n= 35. Error bars represent standard deviation.

(D) Insulin tolerance test (ITT) in DM and healthy controls. Healthy, n = 5; DM, n= 10. Error bars represent standard deviation.

(E) Intraperitoneal glucose tolerance test (iPGTT) in DM and healthy controls. Healthy, n = 9; DM, n= 12. Error bars represent standard deviation.

(F-H) Serum triglyceride, cholesterol, free fatty acid and insulin levels in DM mice and healthy controls. Healthy, n = 7; DM, n= 8. Error bars represent standard deviation.

(I) Serum insulin levels in DM mice and healthy controls. Healthy, n = 5; DM, n= 10. Error bars represent standard deviation.

Statistics: (B-I) unpaired t-test; ****: $p < 0.0001$, ***: $p < 0.0005$, **: $p < 0.005$, *: $p < 0.05$. A non-significant p-value was not indicated in the plots.

Figure 2

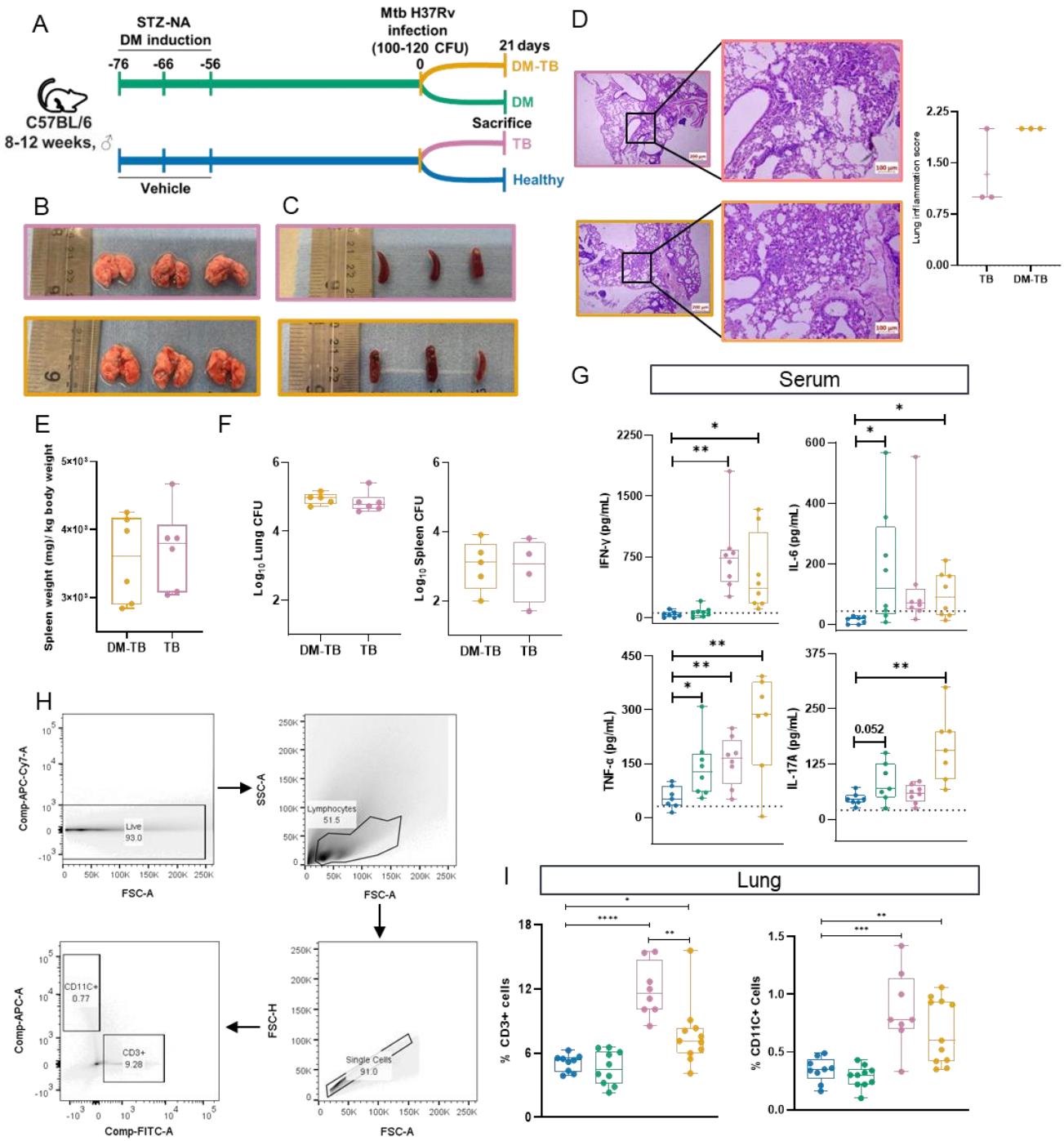

Figure 2: At 21 days post-Mtb H37Rv infection, hyperglycemic (DM) mice and DM-TB mice display comparable tissue bacterial loads to Mtb infected (TB) group with distinct serum cytokine and lung immune cell profiles.

(A) Schematic representation of the experimental plan.

(B, C) Gross lung and spleen pathology in Mtb H37Rv infected mice at 21 days post-infection (d.p.i.).

(D) Hematoxylin and Eosin-stained lung tissue sections show histopathology differences and lung inflammation scores between groups. TB, n = 3; DM-TB, n = 3. Error bars represent standard deviation.

(E) Spleen weight at 21 d.p.i. in DM-TB and TB mice. TB, n = 6; DM-TB, n = 6. Error bars represent standard deviation.

(F) Lung and spleen bacterial burden at 21 d.p.i. in DM-TB and TB mice. TB, n = 6; DM-TB, n= 5 for lung CFU. TB, n = 4; DM-TB, n = 5 for spleen CFU. Error bars represent standard deviation.

(G) Serum IFN-γ, Il-6, TNF-α and Il-17A levels (pg/mL) measured via LEGENDplex assay in healthy, DM, TB and DM-TB groups at 21 d.p.i. Healthy, n = 7; DM, n = 8; TB, n = 8; DM-TB, n = 8 for IFN-γ and IL-6. Healthy, n = 7; DM, n = 8; TB, n = 8; DM-TB, n = 7 for TNF-α and Il-17A. Error bars represent standard deviation.

(H) The gating strategy was used to sort lung CD3+ and CD11C+ cells from all study groups. A representative sample from the TB group is used.

(I) Frequency (%) CD3+ and (B) CD11C+ cells in healthy, DM, TB and DM-TB mice at 21 d.p.i. Healthy, n = 9; DM, n = 10; TB, n = 8; DM-TB, n = 11. Error bars represent standard deviation.

Statistics: (D-I) unpaired t-test; ****: $p < 0.0001$, ***: $p < 0.0005$, **: $p < 0.005$, *: $p < 0.05$. A non-significant p-value was not indicated in the plots.

Figure 3

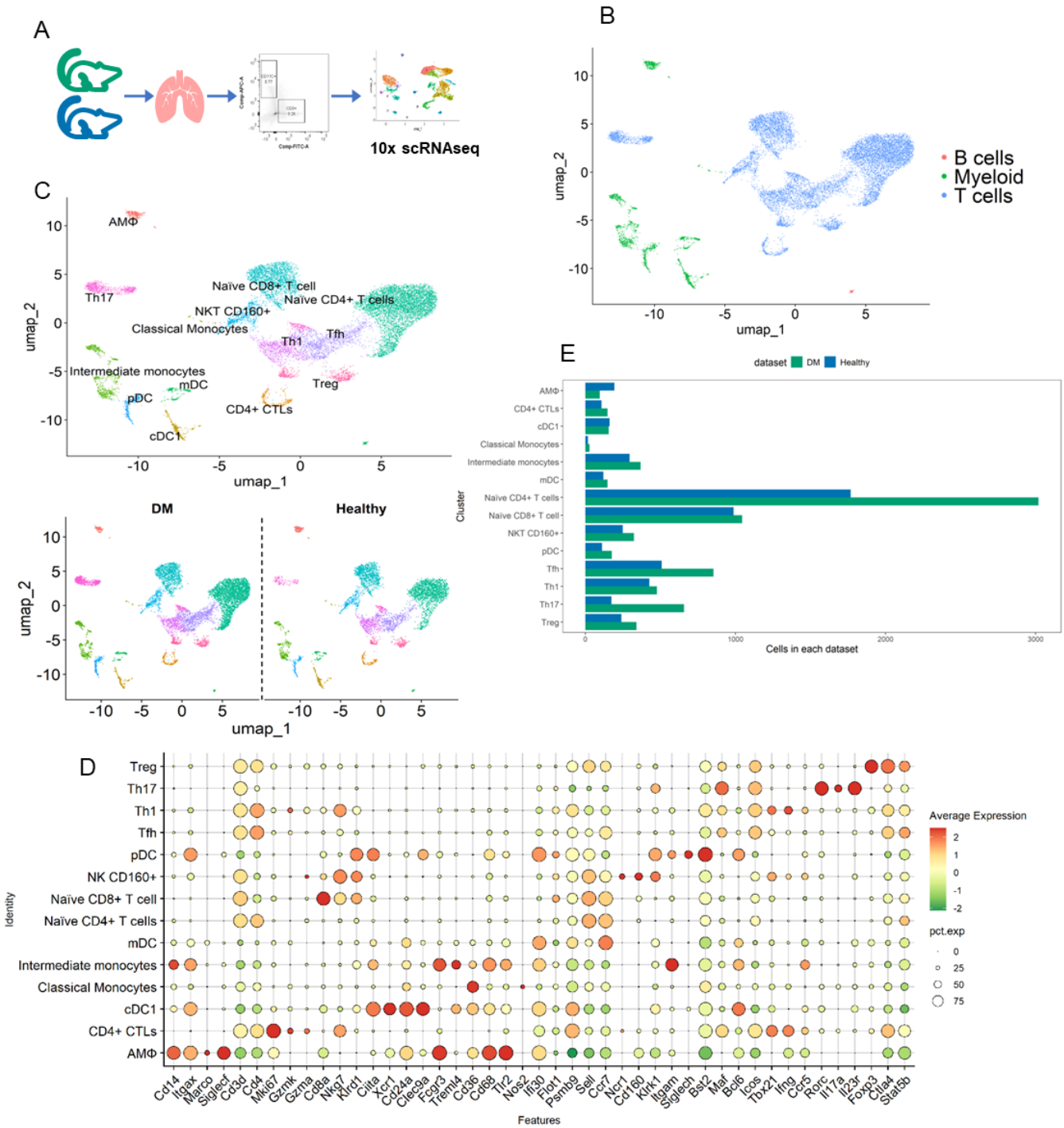

Figure 3: scRNA-seq analysis shows marked alterations in the lung immune cell profiles of diabetic mice.

(A) Schematic representation of the experimental plan.

(B) Uniform Manifold Approximation and Projection (UMAP) visualization of the major cell types representing lymphoid/myeloid cells in dataset.

(C) Annotated UMAP showing lung immune cell subtypes in DM and Healthy mice.

(D) Dot plot indicating expression of key genes detected for each cell subtype.

(E) A stacked bar plot shows the percentage of cell subtypes in each group.

Figure 4

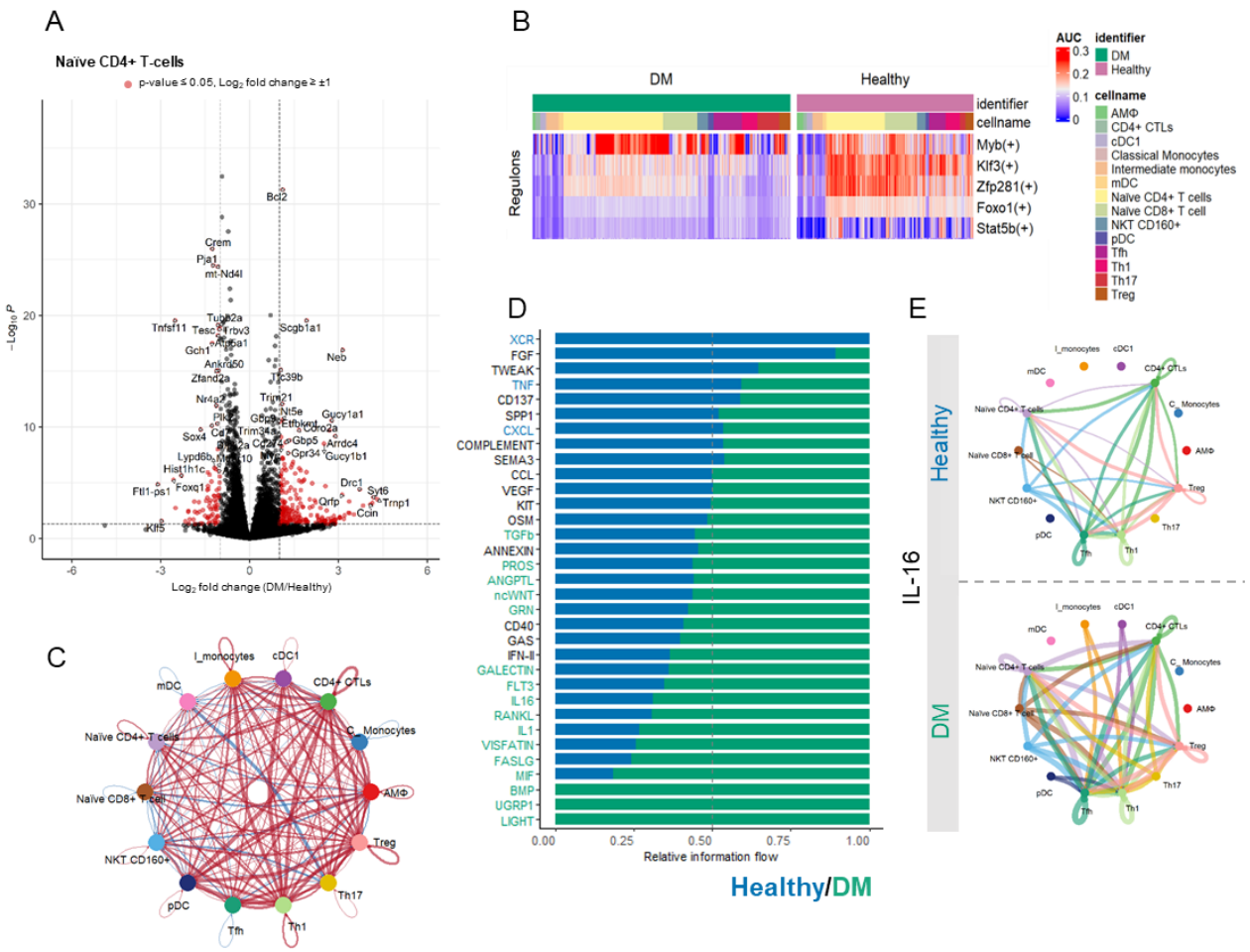

Figure 4: Altered functional, transcriptional, and intercellular communication profiles in lung immune cells of diabetic mice.

(A) Volcano plot showing significantly up-/down-regulated genes in naïve $CD4^+$ T-cells between DM and healthy mice. Significantly deregulated genes: p-value ≤ 0.05, log_2fold change ≥ ± 1.

(B) Heat map showing a subset of differentially activated regulon for cell clusters in hyperglycemic (DM) and euglycemic (healthy) groups. An unpaired Wilcoxon rank-sum test was performed to compare the activity of each regulon between datasets (healthy and DM). p-value ≤ 0.05 was selected for finding the significant difference in regulon activity.

(C) CellChat circle plot showing signalling networks in DM versus healthy groups. The thickness of the edge represents the strength of signalling, and the red and blue colour represent upregulated and downregulated interaction, respectively, in the DM group compared to the healthy control.

(D) A stacked bar plot showing the relative information flow between the ligand-receptor pairs in healthy and DM groups. A paired Wilcoxon test was performed to determine whether there was a significant difference in the signalling information flow between healthy and DM groups. The top signalling pathways coloured green are enriched in DM, and those coloured blue are enriched in the healthy group. p-value ≤ 0.05 was selected for finding the significant difference in regulon activity.

(E) CellChat circle plot showing IL-16 signalling network in DM and healthy groups. The thickness of the edge represents the strength of signalling.

Figure 5

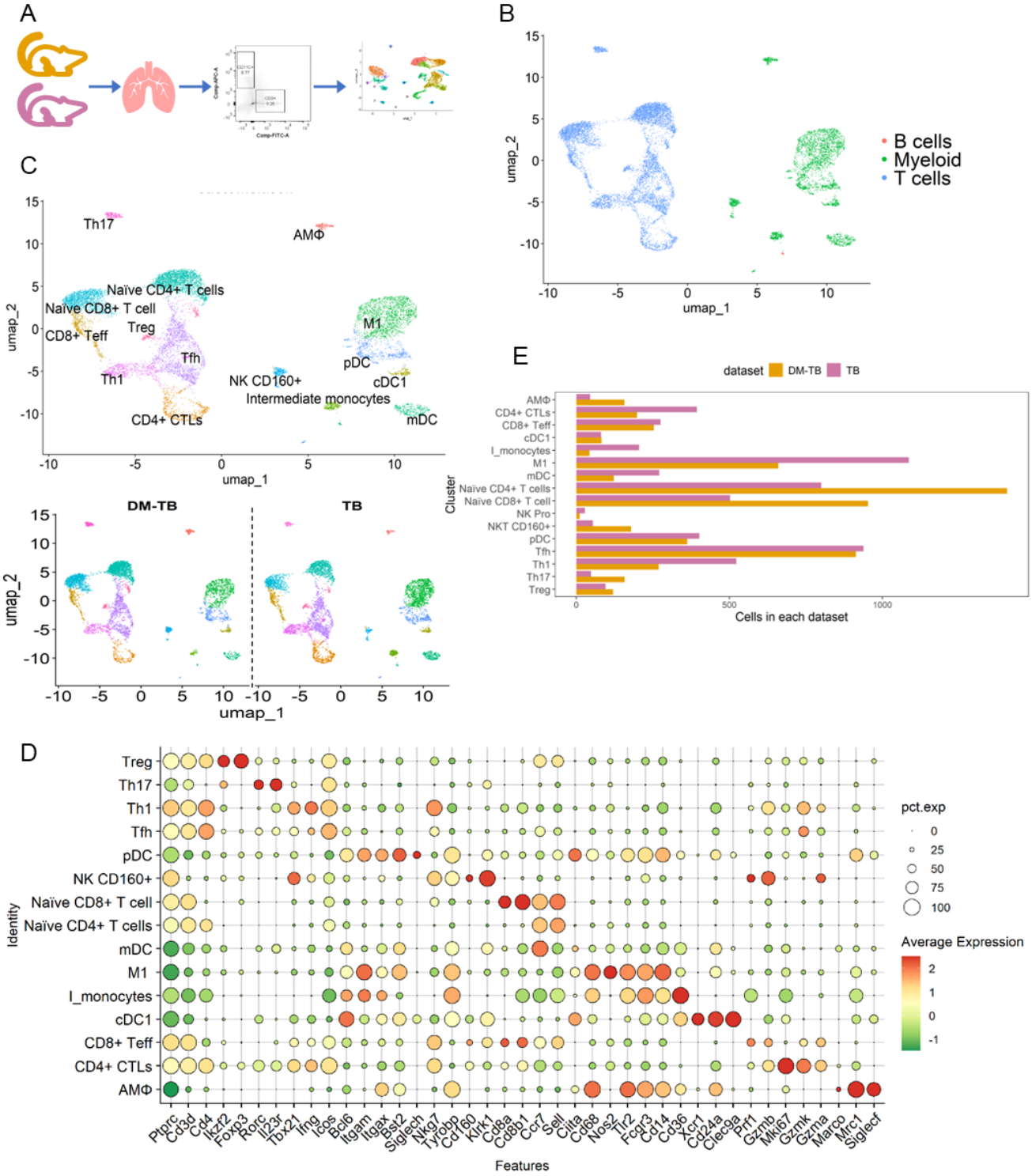

Figure 5: Impact of Mtb H37Rv infection on lung immune cell landscape of diabetic mice.

(A) Schematic representation of the experimental plan.

(B) Uniform Manifold Approximation and Projection (UMAP) visualization of the major cell types representing lymphoid/myeloid cells in the dataset.

(C) Annotated UMAP showing lung immune cell subtypes in DM-TB and TB mice.

(D) Dot plot indicating expression of key genes detected for each cell subtype.

(E) A stacked bar plot shows the percentage of cell subtypes in each group.

Figure 6

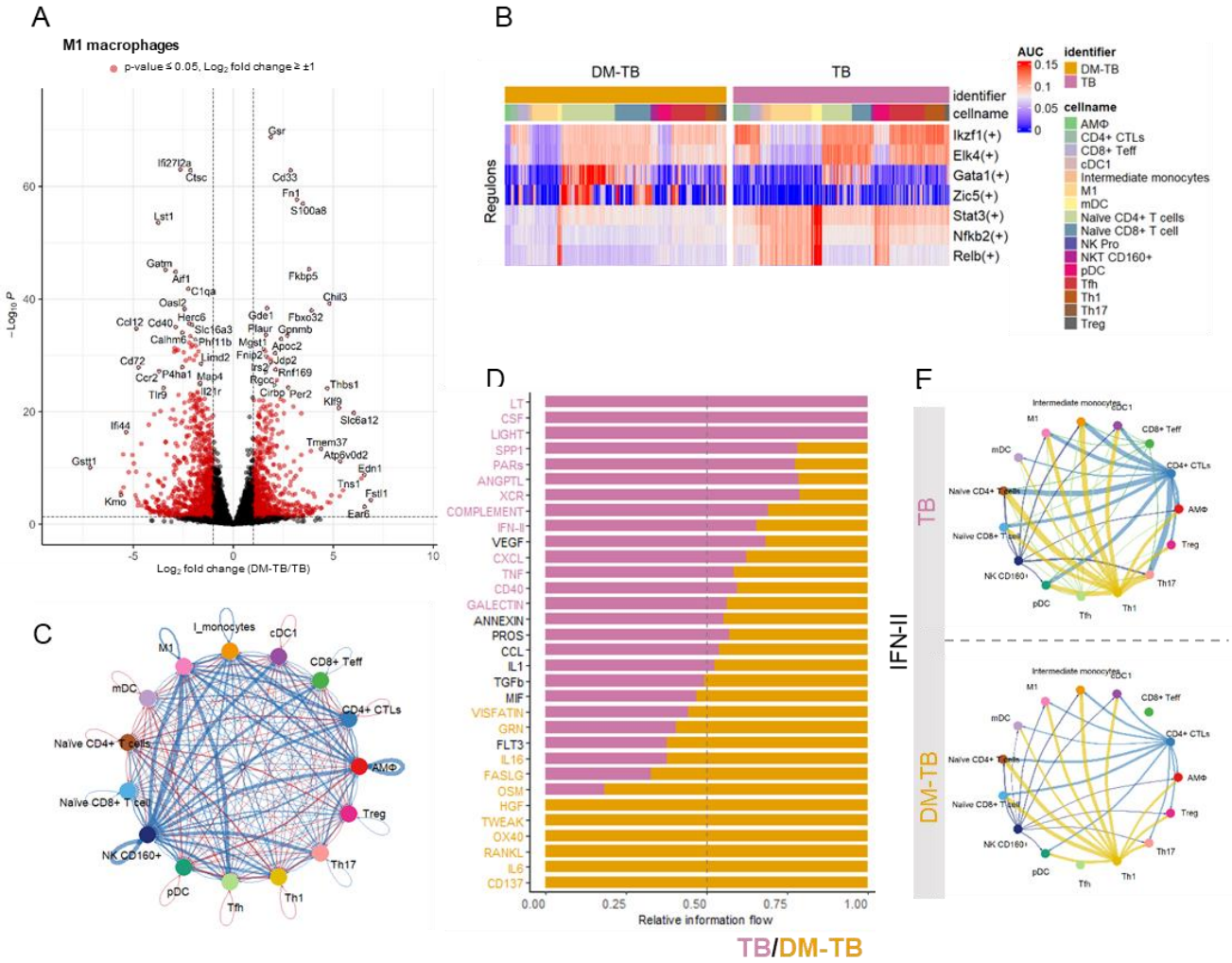

Figure 6: Impaired anti-tuberculosis responses in diabetic mice following Mtb H37Rv infection.

(A) Volcano plot showing significantly up-/down-regulated genes in M1 macrophages between DM-TB and TB mice. Significantly deregulated genes: p-value ≤ 0.05, $\log_2$fold change ≥ ± 1.

(B) Heat map showing a subset differentially activated regulon for cell clusters in the DM-TB and TB groups. An unpaired Wilcoxon rank-sum test was performed to compare the activity of each regulon between datasets (TB and DM-TB). Significant difference in regulon activity: p-value ≤ 0.05.

(C) CellChat circle plot showing signalling networks in DM-TB and TB groups. The thickness of the edge represents the strength of signalling, and the red and blue colours represent upregulated and downregulated interaction, respectively, in the DM-TB group compared to the TB control.

(D) A stacked bar plot showing relative information flow between ligand-receptor pairs in the DM-TB and TB groups. Paired Wilcoxon test was performed to determine whether there was a significant difference in the signalling information flow between healthy and DM groups. The top signalling pathways coloured yellow are enriched in DM-TB, and those coloured pink are enriched in the TB group. Significant difference in information flow: p-value ≤ 0.05.

(E) CellChat circle plot showing IFN-II signalling network in DM-TB and TB groups. The thickness of the edge represents the strength of signalling.

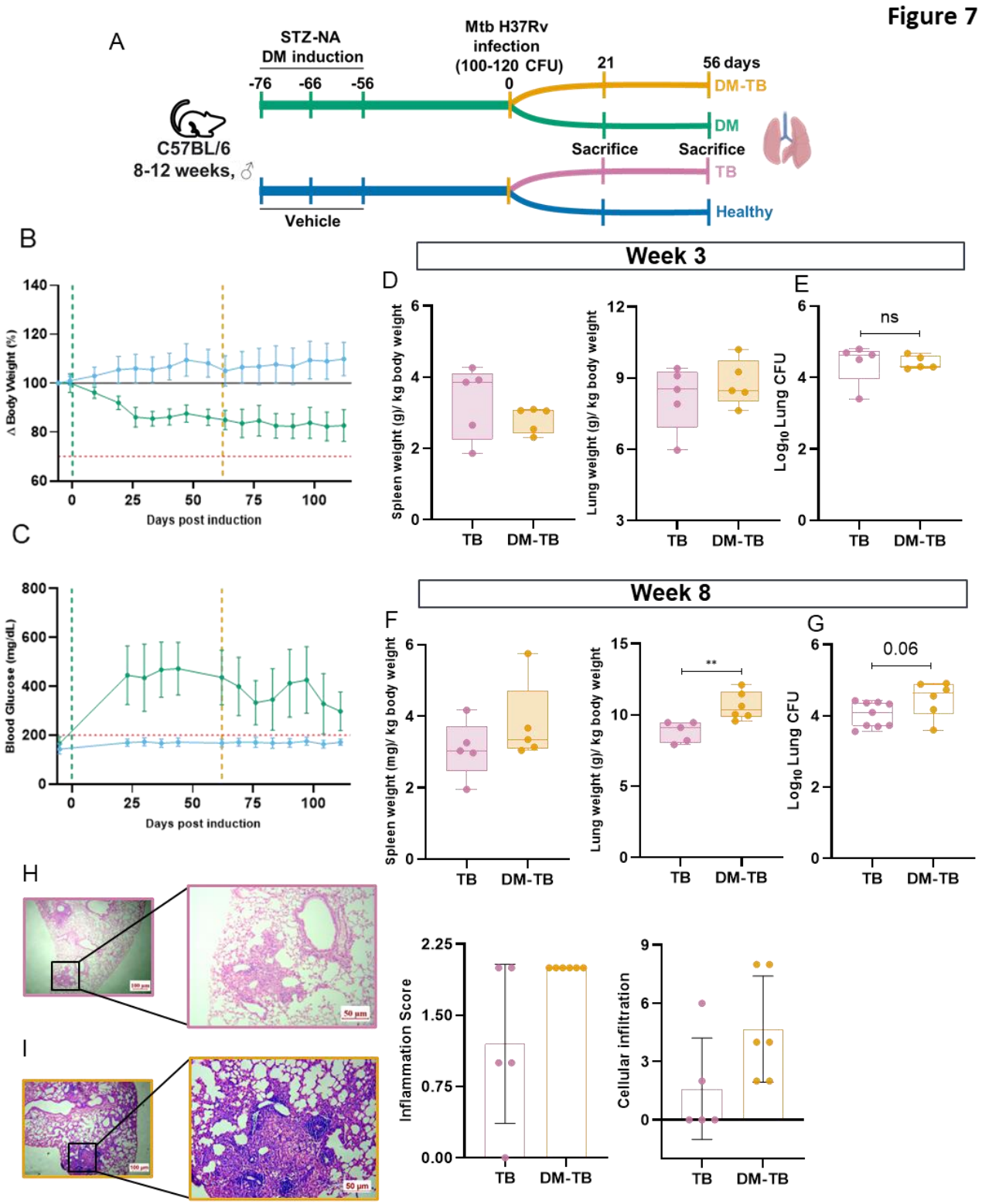

Figure 7: Chronic Mtb H37Rv infection in diabetic mice increases bacterial burden and worsens tissue pathology.

A) Schematic representation of the experimental plan.

(B) Body weight change in DM and healthy mice during the course of the experiment. Healthy, n = 20; DM, n= 11. Error bars represent standard deviation.

(C) Fasting blood glucose levels in diabetic mellitus (DM) mice and healthy controls during the experiment. Healthy, n = 15; DM, n= 21. Error bars represent standard deviation.

(D) Spleen and lung weight in TB and DM-TB groups at 3 weeks post-infection. TB, n = 5; DM-TB, n= 5. Error bars represent standard deviation.

(E) Lung mycobacterial burden in TB and DM-TB groups at 3 weeks post-infection. TB, n = 5; DM-TB, n= 5. Error bars represent standard deviation.

(F) Spleen and lung weight in TB and DM-TB groups at 8 weeks post-infection. TB, n = 5; DM-TB, n= 6. Error bars represent standard deviation.

(G) Lung mycobacterial burden in TB and DM-TB groups at 8 weeks post-infection. TB, n = 9; DM-TB, n= 6. Error bars represent standard deviation.

(H, I) Hematoxylin and Eosin-stained lung tissue sections with inflammation and cellular infiltration scores of TB and DM-TB groups at 8 weeks post-infection.

Statistics: (D-I) unpaired t-test; **: $p < 0.005$., ns: $p > 0.05$ at 95% confidence.